Chapter 8

Modelling the Effect of Fear and Hunting Cooperation in a Prey-predator System with Cooperation and Anti-predation Response Delay

8.1 Introduction

Hunting is the most common phenomenon associated with the survival of all living beings. It connects all the components of multispecies food webs that play a vital role to make nature stable and ecologically balanced. Mathematical models are very useful tool to describe the dynamical behavior of interaction of two or more species. Understanding of ecology with mathematical models begun in the mid of 1920s with two independent works [132, 217]. Since then ecologists are continuously in practice with numerous models considering essential aspects. In 1959, Holling [85] considered the consumption rate of prey by predator (functional response) as a nonlinear function of prey that saturates a certain level. On later it was considered as a function of both prey and predator by some researchers [38]. There are a lot of aspects that are widely studied during the last few decades including conservation and harvesting policies for species, complexity of habitat, Allee effect, stage-structured models, additional food provided to predators, etc.

Group hunting (hunting cooperation) is a vital characteristic among predator species that occurs when more than one predator individuals hunt on a common victim. There are several famous examples of group hunting in mammals including spotted hyena *Crocutta crocutta* [105, 143, 84], African wild dogs *Lycaon pictus* [60, 35], wolves *Canis lupus* [141, 141, 151], chimpanzees *Pan troglodytes* [22, 212], in birds *Aves* [83] and in spiders *Carnivore* [213]. Fanshawe and Fitzgibbon [60] have carried out an experimental study and shown that the success rate of African wild dogs influenced by the age (stage) of prey and the number of members in their pack. The larger group reduces intrspecific interference from other predators like spotted hyena. As a pack, African wild dogs have a success rate per chase of over 85% and a

mean time of only 25 minutes between starting an activity cycle to capturing prey [58]. Chimpanzees are also dependent on small size mammals like colobinae subfamily for meat when fruits become scarce [212]. Boesch [21] studied some cooperative roles (driver, blocker, chaser and ambusher) of Tai chimpanzees during hunting and concluded that chimpanzees are strongly dependent on the cooperative effort by other individuals. There are a lot of research paper available in literature that demonstrates the success rate (percentage of encounters that end with kill) increases in communal hunting. Kruuk [105] has shown that spotted hyena succeeded in 15% of solo hunt of wildebeest *Connochaetes taurinus* calves but it increases up to 74% during group hunts. Even lions *Panthera leo* are not an exception to group hunting, they hunt on Thomson's gazelle *Eudorcas thomsonii* succeeded in 15% of solitary attack but in 32% of communal attack [188]. A book written on spotted hyena [105] reveals that group hunts of some prey species like wildebeest, are significantly more successful than the hunts performed by a lone hyena. Apart from this, there are some other advantages that seem reasonable in group hunting like searching time and chasing distance decreases, hunting probability of huge size prey increases [105], the predators can employ several tactics like making trap or skirmish. Predator individuals deliver some kind of signals for example vocal cues [58], olfactory signals, visual cues [141] that help them to connect with each other while hunting. They have to do this without informing the victim individual. Estes and Goddard [58] have studied that African wild dogs use a repeated bell-like "hoo" as a contact call when the group members are separated.

Recently, few authors have paid attention to analyze the effect of group hunting through modelling and obtain significant results [7, 163]. Alves and Hilker [7] considered a model with Allee effect and hunting cooperation, they found that hunting cooperation is beneficial for predator population due to increasing the capture rate. Saha and Samanta [178] have analyzed an eco-epidemic model with group defense of susceptible prey and hunting cooperation among predators. They revealed the fact that the growth of predators starts decreasing at higher cooperative hunting rate. Possibly, it happens due to the fact that higher cooperation among predators leads to over-exploitation of prey resources and as consequences they face the negative effect.

Since when the models proposed by Lotka and Volterra, the general perspective of explorers was that the predator removes the prey population only by direct killing because it is easy to observe in field. But in recent, some experimantalists have shown that fear effect is as important as direct killing of prey [124, 34, 123, 236, 36]. Due to the fear of being killed by predators, prey individuals show anti predator nature in several forms such as reduce foraging time [6], change the living locality [36], adjust reproduction strategies [171], change in vigilance and physiological nature [202, 168] etc. These facts are supported by field works and experiments on invertebrate and aquatic species. A well constructed experimental work was conducted by Zanette *et al.* [236] on songbirds *Passeri* over an entire breeding period. All the bird individuals which were under experiment, protected by predators (direct killing). Fear was induced in

some songbirds by broadcasting pseudo sounds of predators while rest of the population was kept away to hear such sounds. Authors found 40% deceleratation in the number of progeny of scared population in compared to non-scared population of songbirds. In another experiment [6] on mule deer *Odocoileus hemionus*, it is obtained that due to predation risk of mountain lions *Puma concolor* they reduce the grazing time and shows more vigilant behavior at forest edges than in open and forest areas. Due to an acute level of predation fear a victim individual consumes less forage and confined in a small area which give birth to problems like starvation which again leads to the reduction of birth rate and survival of prey population [36]. Some studies show that fear of being hunted may influence the physiological condition of progeny prey and drop harmful impacts on their survival as mature [34, 32].

In the last few years many authors have paid attention to study fear of predators through mathematical models [220, 221, 187, 148, 109, 163, 237]. The first model on fear effect was proposed and analyzed by Wang *et al.* [220]. They found that increment in the cost of fear may alter the direction of Hopf-bifurcation from supercritical to subcritical under a condition. The effect of fear in a stage structured population model with adaptive avoidance of predators is examined by Wang and Zou [221]. They showed the fear interplays with maturation delay between immature prey and mature prey in determining the long-term population dynamics. The mature prey shows strong anti-predator behaviors at large population of predators whereas it shows weak anti-predator behaviors at high costs of fear. A tri-trophic food chain model with effect of fear was studied by Panday *et al.* [164] and observed that the system exhibits chaotic nature for small costs of fear. Further, the chaotic oscillations are controlled by increasing the fear parameters. Kumar and Dubey [109] analyzed a prey-predator model with fear effect and prey refuge and shown that cost of fear is capable to remove the oscillations from the system. They also concluded that the conservation of prey under a threshold level promotes both the prey and predator populations.

It is known that each biological organism takes an amount of time to respond to any action. This amount of time is said to be *delay* in biology. There are various kind of time delays that represent lag in response of a specific action or process such as hunting [196], digestion of food [107], defense in prey population [183], maturation [26, 55], gestation [46, 109], negative feedback [64, 56], etc. Previously, it has been studied that the prey individuals reflect some anti-predation behaviors in the response of fear induced by predators and consequently their reproduction rate reduces. But in the real scenario, the prey population does not exhibit anti-predation responses as immediate as the fear is induced, while it takes an amount of time to recognize the fear and respond to it [165]. Therefore, the impact of fear follows a time lag to reflect in the reproduction rate prey, which is called *anti-predation response delay*. A delayed model shows much realistic dynamics than a non-delayed model. We incorporate the delay in a model through a delay differential equation. Delay differential equations show finer

but complex behavior than ordinary differential equations. A variety of research articles on single and multiple delay are available in the literature [107, 46, 111, 57, 165]. Kundu and Maitra [111] explored the complex dynamics of a 3-D prey-predator model with interspecific cooperation and three discrete delays and observed that each delay is capable to destabilize the system. Delay is used to control chaos or to remove uneven oscillation from the system [172, 195]. Song and Wei [195] introduced time delayed feedback in Chen's system. The authors found that when the delay passes through a threshold level, chaotic nature is converted into stable steady state or a stable limit cycle.

The objective of this chapter is to analyze the complex dynamics of a prey-predator model with the effect of fear and cooperation hunting. Moreover, the impact of anti-predation response delay and cooperation delay is also incorporated in the model to study the complex dynamics of the system. In the next section, we establish the non-delayed and delayed models. In section 8.3, we discuss some preliminary results. Dynamical analysis of non-delayed model is conducted in section 8.4. Section 8.5 is devoted to stability and Hopf-bifurcation of the delayed system. In section 8.6, we present some numerical simulations in the favor of our findings.

8.2 Formulation of mathematical model

We contemplate an ecological system where two biological populations (one is prey and another is predator) survive. We assume that the prey population grows logistically in the absence of predators. This leads us to the following differential equation

$$\frac{dx}{dt} = rx - r_0x - r_1x^2,$$

where x is number of individuals in prey species at time t, r and r_0 are reproduction rate and natural death rate respectively. The parameter r_1 denotes the coefficient of intraspecific competition among preys.

Let y denotes the predator population and according to some recent field experiments, it was observed that due to the fear induced by predators, the reproduction rate reduces in terms of y and cost of fear k. So, the modified form of above is as follows

$$\frac{dx}{dt} = h(k,y)rx - r_0x - r_1x^2,$$

where $h(k,y)$ is known as fear function and $rh(k,y)$ is effective growth rate of prey under fear effect that mainly depends on cost of fear k and y.

Most of the researchers have worked with the fear function $h(k,y) = \frac{1}{1+ky}$, which is represented by red curve in figure 8.1 [220, 163]. Although, it follows all the above properties that a

fear function should do but despite that it is not much realistic. The reason is the sudden fall in the reproduction rate at low population level of predators. This nature can be clearly seen in the zoomed window of the figure. On the other hand, the blue curve decreases slowly at the low population level and gradually falls with increment of predators then approaches zero at high population density. In this chapter, we work with a modified fear function $h(k,y) = \frac{1}{1+ky^2}$, that makes more sense than the previous one. Therefore, under the effect of fear, the prey-predator model takes the following form

$$\begin{aligned} \frac{dx}{dt} &= \frac{1}{1+ky^2} rx - r_0 x - r_1 x^2 - F(x)y, \\ \frac{dy}{dt} &= cF(x)y - \delta y - \delta_1 y^2, \end{aligned} \tag{8.1}$$

where $F(x)$ is functional response of predators and c, $(0 < c < 1)$ is conversion efficiency denoting the fraction of consumed biomass that transferred into predator biomass. δ is natural death rate of predators and δ_1 is coefficient of intraspecific competition among them.

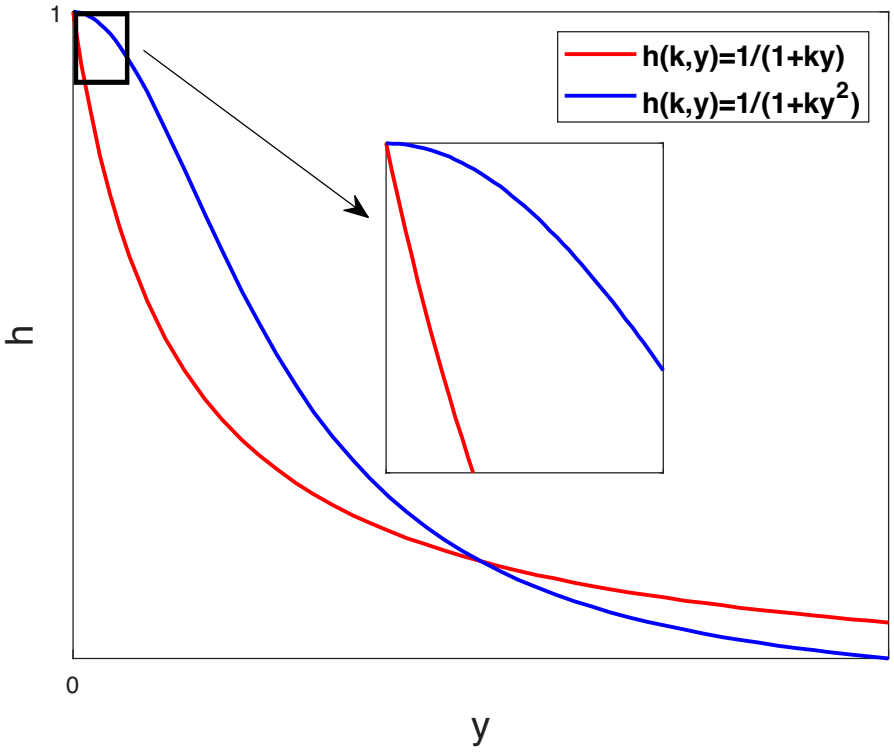

Fig. 8.1: comparison of two types of fear functions.

The functional response or feeding rate is mainly depends on two factors, viz the volume searched for prey per unit time (searching rate or attack rate) and the time taken to consume each prey item (handling time) [85, 153]. According to mass action principle, the feeding rate

always increases linearly with prey density. But in the presence of searching rate and handling time it initially increases and becomes flat at the abundance of prey resources. The Holling type-II functional response is formulated as

$$F(x) = \frac{\alpha x}{1 + a\alpha x},$$

where α is searching rate or attack rate and a is handling time. As we discussed in the previous section, most of small size predators prefer to hunt in packs to boost their hunting success rate. Now, to incorporate the effect of team hunting in the model, we adopt the Berec's perspective of encounter-driven functional response for cooperative behavior among predators [13]. It is based on that the attack rate of predator population increases with predator density and handling time remains constant. Mathematically, the attack rate can be modelled as

$$\alpha(y) = \alpha_0(1+ey)^w, \;\; a(y) = a, \;\; e \geq 0, \;\; w > 0.$$

In this particular study, we choose $w = 1$ so $\alpha(y) = \alpha_0(1+ey) = (\mu + \nu y)$, where $\mu = \alpha_0$ and $\nu = e\alpha_0$. Hence, the modified Holling type-II functional response with cooperative behavior among predators (Berec's encounter-driven functional response) is given as

$$F(x,y) = \frac{(\mu + \nu y)x}{1 + a(\mu + \nu y)x},$$

where μ is predation rate and ν is cooperation strength of the predators. Incorporating the cooperation behavior of predators in the model (8.1), our mathematical model is governed as follows:

$$\begin{aligned}
\frac{dx}{dt} &= \frac{rx}{1+ky^2} - r_0 x - r_1 x^2 - \frac{(\mu + \nu y)xy}{1 + a(\mu + \nu y)x} =: f(x,y), \\
\frac{dy}{dt} &= \frac{c(\mu + \nu y)xy}{1 + a(\mu + \nu y)x} - \delta y - \delta_1 y^2 =: g(x,y), \\
x(0) &= x_0 \geq 0, \; y(0) = y_0 \geq 0.
\end{aligned} \tag{8.2}$$

As previously discussed, predators use several communicational cues to being unified while hunting. But they do not come together in a group as soon as the prey appears, even they need an amount of time to transmit signals and form a group [162]. Due to this, there occurs a time lag in the system that may affect the dynamics. So, it is very reasonable to incorporate a time delay known as cooperation delay τ_2 representing the delay in group forming. In the presence of anti-predation response delay τ_1, the fear function becomes $h(k,y) = \frac{1}{1+ky^2(t-\tau_1)}$. With the

incorporation of both the delays model (8.2) takes the following form

$$\begin{aligned}\frac{dx}{dt} &= \frac{rx}{1+ky^2(t-\tau_1)} - r_0x - r_1x^2 - \frac{(\mu+\nu y(t-\tau_2))xy}{1+a(\mu+\nu y(t-\tau_2))x},\\ \frac{dy}{dt} &= \frac{c(\mu+\nu y(t-\tau_2))xy}{1+a(\mu+\nu y(t-\tau_2))x} - \delta y - \delta_1 y^2,\end{aligned} \tag{8.3}$$

subject to the non negative conditions $x(s) = \phi_1(s) \geq 0,\ y(s) = \phi_2(s) \geq 0,\ s \in [-\tau, 0]$, where $\phi_i(s) \in C([-\tau,0] \to R_+),\ (i = 1,2)$ and $\tau = \max\{\tau_1, \tau_2\}$.

8.3 Preliminaries

For a population model, it is mandatory to examine its well-posedness before moving ahead. Positivity of solution shows that species exist and they never cross zero population level and boundedness illustrates a natural restriction on species to grow them rapidly in the consequences of limited resources. The model (8.2) can be written as

$$\frac{dx}{dt} = x\phi_1(x,y), \quad \frac{dy}{dt} = y\phi_2(x,y),$$

where

$$\phi_1(x,y) = \frac{r}{1+ky^2} - r_0 - r_1x - \frac{(\mu+\nu y)y}{1+a(\mu+\nu y)x}, \quad \phi_2(x,y) = \frac{c(\mu+\nu y)x}{1+a(\mu+\nu y)x} - \delta - \delta_1 y.$$

It follows that

$$x(t) = x(0)e^{\int_0^t \phi_1(x(s),y(s))ds} \geq 0,$$

$$y(t) = y(0)e^{\int_0^t \phi_2(x(s),y(s))ds} \geq 0.$$

Thus, the solution $X(t) = (x(t), y(t))$ with positive initial condition $X(0) = X_0 = (x(0), y(0)) \in R_+^2$ remains positive throughout the region R_+^2.

Theorem 8.3.1. *The set* $\Omega = \{(x,y) : 0 \leq x \leq \frac{r}{r_1}, 0 \leq cx + y \leq \frac{cr^2}{4r_1d}\}$ *is a region of attraction for all solutions initiating in the interior of the positive quadrant, where* $d = min\{r_0, \delta\}$.

Proof. The first equation of model (8.2) implies

$$\frac{dx}{dt} \leq rx - r_1x^2,$$

which implies

$$\limsup_{t\to\infty} x(t) \leq \frac{r}{r_1}.$$

Again let $N(t) = cx(t) + y(t)$,
then we have

$$\frac{dN}{dt} = c\frac{dx}{dt} + \frac{dy}{dt} = \frac{crx}{1+ky^2} - cr_0x - cr_1x^2 - \delta y - \delta_1 y^2 \leq crx - cr_1x^2 - dN,$$

where $d = min\{r_0, \delta\}$.
We also have the maximum value of $crx - cr_1x^2$ is $\frac{cr^2}{4r_1}$ at $x = \frac{r}{2r_1}$. Hence it follows that

$$\limsup_{t\to\infty} N(t) \leq \frac{cr^2}{4r_1 d} =: L.$$

We also note that if $x > \frac{r}{r_1}$ and $y > \frac{cr^2}{4r_1 d}$, then $\frac{dx}{dt} < 0$ and $\frac{dy}{dt} < 0$. This shows that solutions of system (8.2) are bounded and Ω is a positive invariant set. □

Theorem 8.3.2. *Model system (8.2) is uniformly persistence if following inequalities are satisfied:*

$$r > (1+kL^2)(r_0 + (\mu + \nu L)L), \quad \frac{c\mu x_i}{1 + a(\mu + \nu L)x_i} > \delta.$$

Proof. Persistency of a population model illustrates that species will remain for all future time if they are initially exist. Mathematically, the model system (8.2) is said to be uniformly persistent if there are positive constants m and M such that each positive solution $X(t) = (x(t), y(t))$ of the system with positive initial pair satisfies

$$m \leq \liminf_{t\to\infty} X(t) \leq \limsup_{t\to\infty} X(t) \leq M.$$

We define

$$M = max\left\{\frac{r}{r_1}, L\right\},$$

then from Theorem 8.3.1, we have

$$\limsup_{t\to\infty} X(t) \leq M.$$

This also shows that for any sufficiently small $\varepsilon > 0$, there exists a $T > 0$ such that for all $t \geq T$, the following holds:

$$x(t) < \frac{r}{r_1} + \varepsilon, \quad y(t) < Ł + \varepsilon.$$

Now from the first equation of model (8.2), for all $t \geq T$, we can write

$$\frac{dx}{dt} \geq \frac{rx}{1+k(L+\varepsilon)^2} - r_0x - r_1x^2 - (\mu + \nu(L+\varepsilon))(L+\varepsilon)x$$

$$= \left(\frac{r}{1+k(L+\varepsilon)^2} - r_0 - (\mu + \nu(L+\varepsilon))(L+\varepsilon) \right) x - r_1 x^2.$$

It follows that

$$\liminf_{t\to\infty} x(t) \geq \frac{1}{r_1} \left(\frac{r}{1+k(L+\varepsilon)^2} - r_0 - (\mu + \nu(L+\varepsilon))(L+\varepsilon) \right).$$

For sufficiently small $\varepsilon > 0$, we have

$$\liminf_{t\to\infty} x(t) \geq \frac{1}{r_1} \left(\frac{r}{1+kL^2} - r_0 - (\mu + \nu L)L \right) =: x_i.$$

Therefore, the prey population of system (8.2) is persistent under following condition

$$r > (1+kL^2)(r_0 + (\mu + \nu L)L).$$

Now from the second equation of model (8.2), we can write

$$\frac{dy}{dt} \geq \frac{c\mu x_i y}{1+a(\mu+\nu(L+\varepsilon))x_i} - \delta y - \delta_1 y^2$$

$$= \left(\frac{c\mu x_i}{1+a(\mu+\nu(L+\varepsilon))x_i} - \delta \right) y - \delta_1 y^2,$$

which implies

$$\liminf_{t\to\infty} y(t) \geq \frac{1}{\delta_1} \left(\frac{c\mu x_i}{1+a(\mu+\nu(L+\varepsilon))x_i} - \delta \right).$$

For sufficiently small $\varepsilon > 0$, we have

$$\liminf_{t\to\infty} y(t) \geq \frac{1}{\delta_1} \left(\frac{c\mu x_i}{1+a(\mu+\nu L)x_i} - \delta \right) =: y_i.$$

For persistence of the predator population of system (8.2), we must have

$$\frac{c\mu x_i}{1+a(\mu+\nu L)x_i} > \delta.$$

Taking $m = min\{x_i, y_i\}$, the theorem follows. □

8.4 Dynamical behavior of non-delayed model

8.4.1 Existence of equilibrium points

It is investigated that system (8.2) has three equilibria $E_0(0,0), E_1(x_*,0)$ and $E^*(x^*,y^*)$. The trivial equilibrium $E_0(0,0)$ always exists, and $x_* = \frac{1}{r_1}(r-r_0)$. Then $E_1(x_*,0)$ exists if $r > r_0$.

Existence of interior equilibrium $E^*(x^*,y^*)$: The interior equilibria are the positive solutions of the following system of algebraic equations

$$\begin{aligned} &\frac{r}{1+ky^2} - r_0 - r_1 x - \frac{(\mu+\nu y)y}{1+a(\mu+\nu y)x} = 0, \\ &\frac{c(\mu+\nu y)x}{1+a(\mu+\nu y)x} - \delta - \delta_1 y = 0. \end{aligned} \tag{8.4}$$

From the second equation of above system, one can obtain

$$x = \frac{\delta+\delta_1 y}{(c-a(\delta+\delta_1 y))(\mu+\nu y)}.$$

Clearly $x > 0$ if $c > a(\delta+\delta_1 y)$. Now substituting the value of x in the first equation of system (8.4), we get

$$B_0 y^7 + B_1 y^6 + B_2 y^5 + B_3 y^4 + B_4 y^3 + B_5 y^2 + B_6 y + B_7 = 0, \tag{8.5}$$

where

$B_0 = -a^2\delta_1^2 k\nu^2$, $B_1 = 2a\delta_1 k\nu(\nu(c-a\delta) - a\delta_1\mu)$,

$B_2 = 4a\delta_1 k\nu\mu(c-a\delta) - k\nu^2(c-a\delta) - a^2\delta_1^2(\nu^2+k\mu^2)$,

$B_3 = 2a\delta_1(\nu^2+k\mu^2)(c-a\delta) + ac\delta_1 k\nu r_0 - 2a^2\delta_1^2\mu\nu - 2k\mu\nu(c-a\delta)^2$,

$B_4 = ac\delta_1 k\mu r_0 - c\delta_1 k r_1 - a^2\delta_1^2\mu^2 - ck\nu r_0(c-a\delta) - (\nu^2+k\mu^2)(c-a\delta)^2 + 4a\delta_1\mu\nu(c-a\delta)$,

$B_5 = ac\delta_1\nu r_0 - ac\delta_1\nu r - c\delta k r_1 - 2\nu\mu(c-a\delta)^2 - ck\mu r_0(c-a\delta) + 2a\delta_1\mu^2(c-a\delta)$,

$B_6 = c\nu r(c-a\delta) - c\delta_1 r_1 - c\nu r_0(c-a\delta) - \mu^2(c-a\delta)^2 - ac\delta_1\mu(r-r_0)$,

$B_7 = -c\delta r_1 + \mu(c-a\delta)(r-r_0)$.

From equation (8.5), it can be seen that system (8.2) may exhibit at most 7 interior equilibria. The exact number of interior equilibrium point can be obtained by putting certain parametric conditions on the coefficients of equation (8.5). But they seem quite complex and it is difficult

to provide any parametric condition on the coefficients analytically. Here we shall show that how the birth rate of prey population r influences the number of positive equilibrium point. Let's consider the following set of parameters:

$$\begin{aligned} &r_0 = 0.5, \quad r_1 = 0.005, \quad k = 0.006, \quad \mu = 0.75, \quad \nu = 0.2, \\ &a = 0.11, \quad c = 0.3, \quad \delta = 1.68, \quad \delta_1 = 0.1. \end{aligned} \tag{8.6}$$

For the above set of parameters, our observations are listed in Table 8.1. From the biological point of view, it is important to study the uniqueness of interior equilibrium point. Here we are also able to get some conditions on parameters for the existence of a unique positive equilibrium. From the first equation of system (8.4), we note the following:

- When $y = 0$, then $x = \frac{r-r_0}{r_1} =: x_* > 0$.
- When $x = 0$, then $\frac{r}{1+ky^2} - r_0 - (\mu + \nu y)y = 0$, which yields

$$k\nu y^4 + k\mu y^3 + (\nu + r_0 k)y^2 + \mu y - (r - r_0) = 0. \tag{8.7}$$

  Equation (8.7) has always has a unique positive root y_*(say).

- Let's consider a continuously differentiable function $H : R^2 \to R$ such that

$$H(x,y) = \frac{r}{1+ky^2} - r_0 - r_1 x - \frac{(\mu + \nu y)y}{1 + a(\mu + \nu y)x}.$$

  Then we have

$$\frac{\partial H}{\partial y} = -\frac{2rky}{(1+ky^2)^2} - \frac{\mu + 2\nu y + a(\mu + \nu y)^2 x}{(1 + a(\mu + \nu y)x)^2}.$$

  It is observed that $\frac{\partial H}{\partial y} < 0$ for all $(x,y) \in R^2_+$. Hence by the Implicit Function Theorem, $H(x,y) = 0$ can be represented as a continuous function y of x in the interior of the first quadrant.

Table 8.1: Dependence of total number of interior equilibrium points and their stability on parameters r, k, μ and ν. Rest of the parameters are same as in (8.6).

Value of parameters	No. of interior equilibrium points	Equilibrium points	Stability nature
$r = 0.55$	0	-	-
$r = 0.65$	1	(19.073811,0.18362)	stable focus
$r = 2$	1	(77.598227,6.855034)	unstable focus
		(112.234169,9.673778)	saddle point
$r = 2.8447$	2	(21.521139,5.322634)	unstable focus
		(22.813979,5.740728)	unstable focus
$r = 3$	3	(67.940677,9.1256)	saddle point
		(173.787471,9.962255)	stable focus
		(14.360925,4.397571)	unstable focus
$r = 3,\ k = 0.005,\ \mu = 0.01$	4	(76.560757,9.830711)	saddle point
		(202.705685,10.236283)	stable node
		(499.908615,0.0386953)	saddle point
		(33.328355,7.531355)	unstable node
$r = 3.35$	2	(239.923444,10.104824)	stable focus
$r = 4$	1	(337.611621,10.212256)	stable focus
$r = 4.5$	1	(406.201711,10.256567)	stable node

Similarly from the second equation of system (8.4), we can deduce

- When $y = 0$, then $x = \frac{\delta}{(c-\delta a)\mu} =: x_1$.
- When $x = 0$, then $y = -\frac{\delta}{\delta_1} =: y_1 < 0$.
- The slope of the curve is

$$\frac{dy}{dx} = \frac{\frac{c(\mu+\nu y)}{(1+a(\mu+\nu y)x)^2}}{\delta_1 - \frac{c\nu x}{(1+a(\mu+nuy)x)^2}}.$$

It can be noted that the slope $\frac{dy}{dx}$ is positive if $\delta_1 > \frac{c\nu r}{r_1}$.

From the above discussion it is concluded that the graph of the first equation of the system (8.4) enters in the first quadrant through intersecting the $y-$axis at $(0, y^*)$ and behaves as a

continuous function in the interior of the first quadrant and then it enters in the fourth quadrant through intersecting the $x-$axis at the point $(x^*,0)$. The second curve of the system (8.4) passes through $(0,y_1)$ and $(x_1,0)$ and it increases if $a\mu\delta_1 > c\nu$ holds. We also assume that $x_1 < x^*$ to intersect both the curves in the first quadrant.

Theorem 8.4.1. *The interior equilibrium point (x^*,y^*) exists uniquely under the following conditions*

$$a\mu\delta_1 > c\nu \;\; and \;\; x_1 < x^*.$$

8.4.2 Stability analysis

The local nature of a nonlinear system in a vicinity of a point can be approximated by the nature of corresponding Jacobian system. Hence, in order to analyze the local stability nature of existing equilibria we compute the Jacobian matrix and evaluate at each equilibrium point. The analysis follows:

- The equilibrium point $E_0(0,0)$ is always a saddle point.
- The Jacobian matrix, computed at $E_1(x_*,0)$ is

$$J|_{E_1(x_*,0)} = \begin{bmatrix} -(r-r_0) & -\frac{\mu x_*}{1+a\mu x_*} \\ 0 & \frac{c\mu x_*}{1+a\mu x_*} - \delta \end{bmatrix}.$$

  It is noted that the equilibrium point $E_1(x_*,0)$ is

  - locally asymptotically stable if

$$\frac{c\mu x_*}{1+a\mu x_*} < \delta. \tag{8.8}$$

  - saddle point having stable manifold along the $x-$axis and unstable manifold along the $y-$axis if

$$\frac{c\mu x_*}{1+a\mu x_*} > \delta.$$

- The Jaxobian matrix, computed at positive equilibrium $E^*(x^*,y^*)$ is given by

$$J|_{E^*(x^*,y^*)} = \begin{bmatrix} -\left(r_1x^* - \frac{a(\mu+\nu y^*)^2x^*y^*}{(1+a(\mu+\nu y^*)x^*)^2}\right) & -\left(\frac{2rkx^*y^*}{(1+ky^{*2})^2} + \frac{\nu x^*y^*}{(1+a(\mu+\nu y^*)x^*)^2} + \frac{(\mu+\nu y^*)x^*}{(1+a(\mu+\nu y^*)x^*)}\right) \\ \frac{c(\mu+\nu y^*)y^*}{(1+a(\mu+\nu y^*)x^*)^2} & -\left(\delta_1 y^* - \frac{c\nu x^*y^*}{(1+a(\mu+\nu y^*)x^*)^2}\right) \end{bmatrix}.$$

  The characteristic equation corresponding to above Jacobian matrix is

$$\lambda^2 + A_1\lambda + A_2 = 0, \tag{8.9}$$

where

$$A_1 = -tr(J|_{E^*(x^*,y^*)}) = r_1x^* - \frac{a(\mu+\nu y^*)^2x^*y^*}{(1+a(\mu+\nu y^*)x^*)^2} + \delta_1 y^* - \frac{c\nu x^*y^*}{(1+a(\mu+\nu y^*)x^*)^2},$$

$$A_2 = det(J|_{E^*(x^*,y^*)}) = \left(r_1x^* - \frac{a(\mu+\nu y^*)^2x^*y^*}{(1+a(\mu+\nu y^*)x^*)^2}\right)\left(\delta_1 y^* - \frac{c\nu x^*y^*}{(1+a(\mu+\nu y^*)x^*)^2}\right)$$
$$+\frac{c(\mu+\nu y^*)y^*}{(1+a(\mu+\nu y^*)x^*)^2}\left(\frac{2rkx^*y^*}{(1+ky^{*2})^2} + \frac{\nu x^*y^*}{(1+a(\mu+\nu y^*)x^*)^2} + \frac{(\mu+\nu y^*)x^*}{(1+a(\mu+\nu y^*)x^*)}\right).$$

Now using the Routh-Hurwitz criterion, both the eigenvalues of $J|_{E^*(x^*,y^*)}$ have negative real part if and only if

$$A_1 > 0, \quad A_2 > 0. \tag{8.10}$$

Thus, we can state the following theorem.

Theorem 8.4.2. *The positive equilibrium point $E^*(x^*,y^*)$ is locally asymptotically stable in the xy−plane if and only if inequalities in (8.10) hold good.*

Remark 8.4.1. *It is easy to note that inequalities in (8.10) hold if*

$$r_1 > \frac{a(\mu+\nu y^*)^2y^*}{(1+a(\mu+\nu y^*)x^*)^2} \quad \textit{and} \quad \delta_1 > \frac{c\nu x^*}{(1+a(\mu+\nu y^*)x^*)^2} \tag{8.11}$$

satisfy.

Hence, we state the following theorem

Theorem 8.4.3. *If inequalities in (8.11) hold, then $E^*(x^*,y^*)$ is locally asymptotically stable in the xy−plane.*

8.4.3 Bifurcation analysis

In this section, we investigate different bifurcations that system (8.2) exhibits. We obtain the threshold values of parameters where bifurcation occurs and examine the transversility conditions for each bifurcation. In the characteristic equation (8.9) if $A_2 < 0$, then both the eigenvalues are real and have opposite sign. Thus, the following theorem can be stated.

Theorem 8.4.4. *If $A_2 < 0$ then the positive equilibrium $E^*(x^*,y^*)$ is a saddle point.*

Again if $A_1 < 0$ and $A_2 > 0$, then both the eigenvalues are either real and positive or complex conjugate with positive real part. This leads us to the following theorem.

Theorem 8.4.5. *If $A_1 < 0$ and $A_2 > 0$, then the positive equilibrium $E^*(x^*,y^*)$ is unstable.*

From above discussion, if $A_2 > 0$ then the positive equilibrium point $E^*(x^*, y^*)$ switches its stability nature at $A_1 = 0$, where both eigenvalues are purely imaginary. Hence to show the occurrence of Hopf-bifurcation and existence of periodic solutions, we assume $A_1 = 0$ and $A_2 > 0$ that gives the threshold value of parameter $k = k^{[Hf]}$ as

$$k^{[Hf]} = \frac{r - G}{Gy^{*2}}, \tag{8.12}$$

where

$$G = r_0 + 2r_1x^* + \frac{(\mu + \nu y^*)y^*}{(1 + a(\mu + \nu y^*)x^*)^2} - \frac{cx^*(\mu + \nu y^*)(1 + a(\mu + \nu y^*)x^*) + c\nu x^*y^*}{(1 + a(\mu + \nu y^*)x^*)^2} + \delta + 2\delta_1 y^*,$$

and $r > G$.

Theorem 8.4.6. *Assume that $A_2 > 0$, then system (8.2) experiences a Hopf-bifurcation with respect to cost of fear k at $k = k^{[Hf]}$ near the positive equilibrium E^*.*

Proof. It can be noted that

(i) If $A_1 > 0$ and $A_2 > 0$, then $k > k^{[Hf]}$ and E^* is locally asymptotically stable.

(ii) If $A_1 < 0$ and $A_2 > 0$, then $k < k^{[Hf]}$ and E^* is unstable.

This shows that E^* switches its stability nature from instability to local asymptotic stability as the cost of fear passes through its threshold value $k = k^{[Hf]}$. We note that at $k = k^{[Hf]}$, $tr(J|_{E^*(x^*,y^*)}) = 0$ but $det(J|_{E^*(x^*,y^*)}) > 0$. Hence the eigenvalues are purely imaginary.

For Hopf-bifurcation the transversality condition also must be satisfied. We have

$$\left[\frac{d}{dk}\left(tr(J|_{E^*})\right)\right]_{k=k^{[Hf]}} = -\frac{ry^{*^2}}{(1 + ky^{*^2})^2} < 0.$$

Hence by the Andronov-Hopf bifurcation theorem, system (8.2) experiences a Hopf-bifurcation with respect to cost of fear k at $k = k^{[Hf]}$ near E^*. □

We can fix some criteria for the existence of periodic orbit of system (8.2) using Poincare-Bendixson Theorem.

Theorem 8.4.7. *Assume $\frac{c\mu x_*}{1+a\mu x_*} > \delta$ and one of the following hold*

(i) $A_2 < 0$,

(ii) $A_1 < 0$ *and* $A_2 > 0$

then the system (8.2) has a limit cycle.

Proof. Earlier, we have shown that the interior of set Ω is a positively invariant set. We have also carried out that if $\frac{c\mu x_*}{1+a\mu x_*} > \delta$ then the axial equilibrium $E_*(x_*,0)$ is a saddle point and if $A_2 < 0$ or $A_1 < 0$ and $A_2 > 0$ then the positive equilibrium is unstable. Thus, the positive limit set does not contain any equilibrium point. Hence by Poincare-Bendixson Theorem, the system must have a limit cycle. □

Theorem 8.4.8. *The system (8.2) experiences a transcritical bifurcation in the axial equilibrium $E_*(\frac{r-r_0}{r_1},0) = E_*(x_*,0)$ and interior equilibrium $E^*(x^*,y^*)$ with respect to the parameter μ at $\mu^{[tc]} = \frac{r_1\delta}{(c-a\delta)(r-r_0)}$ if $c > a\delta$ and $\Delta_3 \neq 0$, where Δ_3 is defined in the proof.*

Proof. The variational matrix of the system (8.2) in the vicinity of the axial equilibrium $E_*(x_*,0)$ is given as

$$J|_{E_*(x_*,0)} = \begin{bmatrix} -(r-r_0) & -\frac{\mu x_*}{1+a\mu x_*} \\ 0 & \frac{c\mu x_*}{1+a\mu x_*} - \delta \end{bmatrix}.$$

One eigenvalue of above matrix is $-(r-r_0)$ and other eigenvalue will be zero if and only if $\mu = \mu^{[tc]}$. At $\mu = \mu^{[tc]}$ the above matrix takes the following form

$$J^{[tc]}|_{E_*(x_*,0)} = \begin{bmatrix} -(r-r_0) & -\frac{\delta}{c} \\ 0 & 0 \end{bmatrix}.$$

The vectors $V = (1, -\frac{(r-r_0)c}{\delta})^T$ and $W = (0,1)^T$ are eigenvectors corresponding to the zero eigenvalue of the matrix $J^{[tc]}|_{E_*(x_*,0)}$ and its transpose matrix respectively. Let $F = (f,g)^T$, where f and g are defined previously. Now we define $\Delta_1 = W^T[F_\mu(E_*,\mu^{[tc]})]$, where F_μ denotes the partial derivative of F with respect to μ. Then we have

$$\Delta_1 = W^T[F_\mu(E_*,\mu^{[tc]})] = (0,1)(0,0)^T = 0.$$

Let $\Delta_2 = W^T[DF_\mu(E_*,\mu^{[tc]})V]$, where

$$DF_\mu(E_*,\mu^{[tc]}) = \begin{bmatrix} 0 & \frac{a\delta^2}{\mu^{[tc]}c^2} - \frac{\delta}{\mu^{[tc]}c} \\ 0 & -\frac{a\delta^2}{\mu^{[tc]}c} + \frac{\delta}{\mu^{[tc]}} \end{bmatrix}.$$

A little calculation yields

$$\Delta_2 = -\frac{(r-r_0)^2(c-a\delta)^2}{r_1\delta} < 0.$$

Again we define $\Delta_3 = W^T[D^2F(E_*,\mu^{[tc]})(V,V)]$, where $D^2F(E_*,\mu^{[tc]})$ is evaluated as

$$D^2F(E_*,\mu^{[tc]}) = \begin{bmatrix} f_{xx} & f_{xy} & f_{yx} & f_{yy} \\ g_{xx} & g_{xy} & g_{yx} & g_{yy} \end{bmatrix},$$

where all the entries in above matrix have the conventional meaning and we calculated at E^* and $\mu = \mu^{[tc]}$ as

$$f_{xx} = -2r_1,\ \ f_{xy} = f_{yx} = -\frac{(c-a\delta)\delta r_1}{c^2(r-r_0)},\ \ f_{yy} = -\frac{2(c-a\delta)\nu\delta}{c^2\mu^{[tc]}} - \frac{2rk(r-r_0)}{r_1},$$

$$g_{xx} = 0,\ \ g_{xy} = g_{yx} = \frac{(c-a\delta)\delta r_1}{c(r-r_0)},\ \ g_{yy} = \frac{2(c-a\delta)\nu\delta}{c\mu^{[tc]}} - 2\delta_1.$$

Putting these values in the expression of Δ_3, one can easily get

$$\Delta_3 = -2(c-a\delta)r_1 + \left(\frac{2\nu(c-a\delta)^2(r-r_0)}{cr_1} - 2\delta_1\right)\frac{(r-r_0)^2c^2}{\delta^2}.$$

If $\Delta_3 \neq 0$ then all the conditions of Sotomayor's Theorem [169] are fulfilled. Thus, the system(8.2) experiences a transcritical bifurcation in the axial equilibrium $E_*(x_*,0)$ and interior equilibrium $E^*(x^*,y^*)$ with respect to the parameter μ at $\mu^{[tc]} = \frac{r_1\delta}{(c-a\delta)(r-r_0)}$. □

Theorem 8.4.9. *The system (8.2) undergoes a saddle node bifurcation around $\bar{E}(\bar{x},\bar{y})$ with respect to the parameter μ at $\mu = \mu^{[sn]}$, if $\Omega_1 \neq 0$ and $\Omega_2 \neq 0$ where $\bar{E}(\bar{x},\bar{y})$ is the equilibrium point when $\mu = \mu^{[sn]}$ at which two interior equilibrium points E_1^* and E_2^* collide, and Ω_1, Ω_2 are defined in the proof.*

Proof. We shall use the Sotomayor's Theorem [169, 209] to show that the system (8.2) undergoes a saddle node bifurcation with respect to the parameter μ. The Jacobian of the system at the equilibrium $\bar{E}(\bar{x},\bar{y})$ is given by

$$\bar{J} = DF(\bar{x},\bar{y}) = \begin{bmatrix} j_{11} & j_{12} \\ j_{21} & j_{22} \end{bmatrix},$$

where

$$j_{11} = -\left(r_1\bar{x} - \frac{a(\mu+\nu\bar{y})^2\bar{x}\bar{y}}{(1+a(\mu+\nu\bar{y})\bar{x})^2}\right),\ \ j_{12} = -\left(\frac{2rk\bar{x}\bar{y}}{(1+k\bar{y}^2)^2} + \frac{\nu\bar{x}\bar{y}}{(1+a(\mu+\nu\bar{y})\bar{x})^2} + \frac{(\mu+\nu\bar{y})\bar{x}}{(1+a(\mu+\nu\bar{y})\bar{x})}\right),$$

$$j_{21} = \frac{c(\mu+\nu\bar{y})\bar{y}}{(1+a(\mu+\nu\bar{y})\bar{x})^2},\ \ j_{22} = -\left(\delta_1\bar{y} - \frac{c\nu\bar{x}\bar{y}}{(1+a(\mu+\nu\bar{y})\bar{x})^2}\right).$$

Let $\mu^{[sn]}$ be the value of μ such that the matrix $\bar{J}$ has a zero eigenvalue. This demands $det(\bar{J}) = 0$ at $\mu = \mu^{[sn]}$. The vectors $V_1 = (1, -\frac{j_{11}}{j_{12}})^T$ and $W_1 = (1, -\frac{j_{11}}{j_{21}})^T$ are the eigenvectors corresponding to the zero eigenvalue of the matrices $\bar{J}$ and $\bar{J}^T$, respectively. Now we define

$\Omega_1 = W_1^T F_\mu(\bar{E}, \mu^{[sn]})$, where $F_\mu(\bar{E}, \mu^{[sn]}) = (f_\mu, g_\mu)^T$ evaluated at $\bar{E}$ and $\mu = \mu^{[sn]}$ as

$$f_\mu = \frac{a\bar{x}^2\bar{y}(\mu^{[sn]} + \nu\bar{y})}{(1+a(\mu^{[sn]} + \nu y)\bar{x})^2} - \frac{\bar{x}\bar{y}}{1+a(\mu^{[sn]} + \nu\bar{y})\bar{x}},\ g_\mu = -\frac{ca\bar{x}^2\bar{y}(\mu^{[sn]} + \nu\bar{y})}{(1+a(\mu^{[sn]} + \nu\bar{y})\bar{x})^2} + \frac{c\bar{x}\bar{y}}{1+a(\mu^{[sn]} + \nu\bar{y})\bar{x}}.$$

Then a simple calculation yields

$$\Omega_1 = f_\mu - \frac{j_{11}}{j_{21}} g_\mu.$$

Again, we define $\Omega_2 = W_1^T D^2 F(\bar{E}, \mu^{[sn]})(V_1, V_1)$, where $D^2F(\bar{E}, \mu^{[sn]})(V_1, V_1)$ is given by

$$D^2F(\bar{E}, \mu^{[sn]})(V_1, V_1) = \begin{bmatrix} f_{xx} - \frac{j_{11}}{j_{12}} f_{xy} - \frac{j_{11}}{j_{12}} f_{yx} + \frac{j_{11}^2}{j_{12}^2} f_{yy} \\ g_{xx} - \frac{j_{11}}{j_{12}} g_{xy} - \frac{j_{11}}{j_{12}} g_{yx} + \frac{j_{11}^2}{j_{12}^2} g_{yy} \end{bmatrix},$$

Then one can easily obtain

$$\Omega_2 = f_{xx} - \frac{j_{11}}{j_{12}} f_{xy} - \frac{j_{11}}{j_{12}} f_{yx} + \frac{j_{11}^2}{j_{12}^2} f_{yy} - \frac{j_{11}}{j_{21}} g_{xx} + \frac{j_{11}^2}{j_{12}j_{21}} g_{xy} + \frac{j_{11}^2}{j_{12}j_{21}} g_{yx} - \frac{j_{11}^3}{j_{12}^2 j_{21}} g_{yy}.$$

Thus from Sotomayor's Theorem, the system (8.2) undergoes a saddle node bifurcation around $\bar{E}(\bar{x}, \bar{y})$ at $\mu = \mu^{[sn]}$ if $\Omega_1 \neq 0$ and $\Omega_2 \neq 0$. □

8.4.4 Global stability

In this section, we shall obtain the criterion of the global asymptotic stability of axial and positive equilibrium points. Global asymptotic stability convey that the basin of attraction of a particular solution is the whole invariant set.

Theorem 8.4.10. *The equilibrium point $E_1(x_*, 0)$ is globally asymptotically stable under following inequality*

$$c(\mu + \nu L)x_* < \delta. \tag{8.13}$$

Proof. We consider a positive definite function

$$\Phi(x, y) = c\Big(x - x_* - x_* \ln\big(\frac{x}{x_*}\big)\Big) + y.$$

The derivative of Φ with respect to time gives

$$\frac{d\Phi}{dt} = c(x - x_*)\Big(\frac{r}{1+ky^2} - r_0 - r_1 x\Big) + \frac{c(\mu + \nu y)yx_*}{1+a(\mu + \nu y)x} - \delta y - \delta_1 y^2.$$

Since $x_* = \frac{r-r_0}{r_1}$, so it follows

$$\frac{d\Phi}{dt} \leq -\frac{c}{r_1}\left(\frac{r}{1+ky^2} - r_0 - r_1 x\right)^2 + \frac{c(\mu+\nu y)yx_*}{1+a(\mu+\nu y)x} - \delta y - \delta_1 y^2.$$

Fro the above, it is easy to note that $\frac{d\Phi}{dt}$ is negative definite under inequality (8.13). Hence, $E_1(x_*,0)$ is globally asymptotically stable under inequality (8.13). □

Theorem 8.4.11. *System (8.2) is globally asymptotically stable around the positive equilibrium point if the following conditions hold:*

$$\gamma > 0, \quad \eta > 0, \quad \textit{and} \quad \zeta^2 < 4\gamma\eta, \tag{8.14}$$

where γ, η, ζ are defined in the proof.

Proof. We consider a positive definite function $\Psi(x,y)$ around the positive equilibrium point (x^*,y^*)

$$\Psi(x,y) = x - x^* - x^* \ln\left(\frac{x}{x^*}\right) + \frac{1}{c}\left(y - y^* - y^* \ln\left(\frac{y}{y^*}\right)\right).$$

Differentiating the above function with respect to time along the solution of the system (8.2), we get

$$\frac{d\Psi}{dt} = \frac{(x-x^*)}{x}\frac{dx}{dt} + \frac{1}{c}\frac{(y-y^*)}{y}\frac{dy}{dt}.$$

A simple mathematical manipulation yields

$$\begin{aligned}\frac{d\Psi}{dt} = &-\left[r_1 - \frac{a\mu^2 y^* + a\mu\nu y^*(y+y^*) + a\nu^2 y^*}{(1+a(\mu+\nu y)x)(1+a(\mu+\nu y^*)x^*)}\right](x-x^*)^2 - \left[\frac{rk(y+y^*)}{(1+ky^2)(1+ky^{*2})}\right.\\ &\left.+ \frac{\nu y^* + a\mu^2 x^* + a\mu x^*\nu(y+y^*) + a\nu^2 x^*}{(1+a(\mu+\nu y)x)(1+a(\mu+\nu y^*)x^*)}\right](x-x^*)(y-y^*)\\ &-\left[\frac{\delta_1}{c} - \frac{\nu x^*}{(1+a(\mu+\nu y)x)(1+a(\mu+\nu y^*)x^*)}\right](y-y^*)^2.\end{aligned}$$

Applying the Sylvester's criterion, $\frac{d\Psi}{dt}$ is negative definite if

$$\gamma > 0, \quad \eta > 0, \quad \text{and} \quad \zeta^2 < 4\gamma\eta,$$

where

$$\gamma = r_1 - \frac{a\mu^2 y^* + a\mu\nu y^*(y^*+L) + a\nu^2 y^*}{1+a(\mu+\nu y^*)x^*}, \quad \eta = \frac{\delta_1}{c} - \frac{\nu x^*}{1+a(\mu+\nu y^*)x^*},$$

$$\zeta = \frac{rk(y^*+L)}{1+ky^{*2}} + \frac{\nu y^* + a\mu^2 x^* + a\mu\nu x^*(y^*+L) + a\nu^2 x^*}{1+a(\mu+\nu y^*)x^*}.$$

Hence, the positive equilibrium point $E^*(x^*, y^*)$ is globally asymptotically stable under condition (8.14). □

8.5 Analysis of delayed model

In this component, we shall explore the local stability of delayed system (8.3) near all the existing equilibrium points. It is known that equilibrium points are not affected by introducing the time delay in the system. The delayed system (8.3) can be written in vector form as follows

$$\frac{dZ}{dt} = \mathcal{G}(Z(t), Z(t-\tau_1), Z(t-\tau_2)), \tag{8.15}$$

where

$$Z(t) = [x(t), y(t)]^T, \text{ and } Z(t-\tau_i) = [x(t-\tau_i), y(t-\tau_i)]^T, \ i = 1, 2.$$

The linearized system of (8.15) around a point (u, v) is given by

$$\frac{dX(t)}{dt} = PX(t) + QX(t-\tau_1) + RX(t-\tau_2),$$

where

$$P = \left[\frac{\partial \mathcal{G}}{\partial Z(t)}\right]_{(u,v)}, \ Q = \left[\frac{\partial \mathcal{G}}{\partial Z(t-\tau_1)}\right]_{(u,v)}, \ R = \left[\frac{\partial \mathcal{G}}{\partial Z(t-\tau_2)}\right]_{(u,v)} \text{ and } X(t) = [x(t)-u, y(t)-v]^T.$$

Hence, the variational matrix of the delayed system (8.3) at the point (u, v) can be given as

$$J^D|_{(u,v)} = \begin{bmatrix} p_{11} & p_{12} + q_{12}e^{-\lambda\tau_1} + r_{12}e^{-\lambda\tau_2} \\ p_{21} & p_{22} + r_{22}e^{-\lambda\tau_2} \end{bmatrix},$$

where

$$p_{11} = \frac{r}{1+kv^2} - r_0 - 2r_1 u - \frac{(\mu+\nu v)v}{(1+a(\mu+\nu v)u)^2}, \ p_{12} = -\frac{u(\mu+\nu v)}{1+a(\mu+\nu v)u}, \ p_{21} = \frac{c(\mu+\nu v)v}{(1+a(\mu+\nu v)u)^2},$$

$$p_{22} = \frac{cu(\mu+\nu v)}{1+a(\mu+\nu v)u} - \delta - 2\delta_1 v, \ q_{12} = -\frac{2rkuv}{(1+kv^2)^2}, \ r_{12} = -\frac{\nu uv}{(1+a(\mu+\nu v)u)^2}, \ r_{22} = -cr_{12}.$$

Remark 8.5.1. *In the above matrix, $q_{12} = r_{12} = r_{22} = 0$ if $u = 0$ or $v = 0$. In such a case, the variational matrix turns out to be same as the non-delayed model. Thus, the delay does not affect the local asymptotic stability of trivial equilibrium point $E_0(0,0)$ and the axial equilibrium*

point $E_*(x_*,0)$.

The characteristic equation of the variational matrix evaluated at the positive equilibrium point $(u,v) = E^*(x^*,y^*)$ is

$$\lambda^2 + d_1\lambda + d_2 + d_3e^{-\lambda\tau_1} + (d_4\lambda + d_5)e^{-\lambda\tau_2} = 0, \tag{8.16}$$

where $d_1 = -(p_{11}+p_{22})$, $d_2 = p_{11}p_{22} - p_{12}p_{21}$, $d_3 = -p_{21}q_{12}$, $d_4 = -r_{22}$, $d_5 = p_{11}r_{22} - p_{21}r_{12}$.

Remark 8.5.2. *When* $\tau_1 = \tau_2 = 0$, *then the equation (8.16) is same as the characteristic equation (8.9) obtained for non-delayed system.*

Case (1): When $\tau_1 > 0$ and $\tau_2 = 0$. In this case the characteristic equation takes the following form

$$\lambda^2 + b_1\lambda + b_2 + d_3e^{-\lambda\tau_1} = 0, \tag{8.17}$$

where $b_1 = d_1 + d_4$, $b_2 = d_2 + d_5$. The system (8.3) is stable near the positive equilibrium point if and only if all the characteristic roots of equation (8.17) have negative real part. For the switching of stability of E^* through Hopf-bifurcation, the characteristic root must intersect the imaginary axis. Therefore, we assume $i\omega$ be a root of equation (8.17). Then splitting the real and imaginary parts, we obtain

$$\begin{aligned} d_3\cos\omega\tau_1 &= \omega^2 - b_2, \\ d_3\sin\omega\tau_1 &= b_1\omega. \end{aligned} \tag{8.18}$$

Squaring and then adding both the equations of (8.18), we get

$$\omega^4 + (b_1^2 - 2b_2)\omega^2 + (b_2^2 - d_3^2) = 0. \tag{8.19}$$

Putting $\omega^2 = z$, above equation becomes

$$h(z) = z^2 + (b_1^2 - 2b_2)z + (b_2^2 - d_3^2) = 0. \tag{8.20}$$

Proposition 8.5.1. *If equation (8.19) does not have any positive root, then the stability nature of* E^* *does not change for all* $\tau_1 \geq 0$.

Remark 8.5.3. *It can be observed that if* $b_1^2 - 2b_2 > 0$ *and* $b_2^2 - d_3^2 > 0$, *then equation (8.19) does not have any positive root, so the stability behavior remains same as the non-delayed system (8.2).*

Theorem 8.5.1. *Assume that inequalities in (8.10) hold and the conditions* $b_2^2 - d_3^2 < 0$ *and* $h'(\omega_0^2) \neq 0$ *are also satisfied. Then there exist a threshold value of* $\tau_1 = \tau_1^{[Hf]}$*, where the delayed system (8.3) experiences a Hopf-bifurcation.*

Proof. Assume that inequalities in (8.10) hold good, then the non-delayed system (8.2) is locally stable around E^*. Again let $b_2^2 - d_3^2 < 0$, so that equation (8.19) have a unique positive root ω_0. On substitution of ω_0 in equation (8.18), we get

$$d_3 \cos \omega_0 \tau_1 = \omega_0^2 - b_2,$$
$$d_3 \sin \omega_0 \tau_1 = b_1 \omega_0.$$

which yields

$$\tau_1^j = \frac{1}{\omega_0} \tan^{-1}\left[\frac{b_1\omega_0}{\omega_0^2 - b_2}\right] + \frac{2j\pi}{\omega_0}, \quad j = 0, 1, 2, \ldots \tag{8.21}$$

We also have

$$\left[\frac{d\lambda}{d\tau_1}\right]^{-1}_{\lambda=i\omega_0} = \frac{b_1 + 2i\omega_0}{i\omega_0 d_3} e^{i\omega_0\tau_1} + \frac{i\tau_1}{\omega_0},$$

which leads

$$Re\left[\frac{d\lambda}{d\tau_1}\right]^{-1}_{\lambda=i\omega_0} = \frac{2\omega_0 \cos\omega_0\tau_1 + b_1 \sin\omega_0\tau_1}{d_3\omega_0}.$$

Using equation (8.20) in the above expression, we obtain

$$Re\left[\frac{d\lambda}{d\tau_1}\right]^{-1}_{\lambda=i\omega_0} = \frac{h'(\omega_0^2)}{d_3^2}.$$

Therefore, the transversility condition holds if $h'(\omega_0^2) \neq 0$. Hence, according to Andronov-Hopf bifurcation theorem, the delayed system (8.3) exhibits Hopf-bifurcation at $\tau_1 = \tau_1^{[Hf]}$. □

Case (2): When $\tau_1 = 0$ and $\tau_2 > 0$. Then the characteristic equation (8.16) becomes

$$\lambda^2 + d_1\lambda + (d_2 + d_3) + (d_4\lambda + d_5 e^{-\lambda\tau_2} = 0, \tag{8.22}$$

One can deduce the following theorem under the analysis similar to the previous case.

Theorem 8.5.2. *Assume that inequalities in (8.10) hold and the condition* $(d_2 + d_3)^2 - d_5^2 < 0$ *is also satisfied. Then the delayed system (8.3) experiences a Hopf-bifurcation at* $\tau_2 = \tau_2^{[Hf]}$*, given by*

$$\tau_2^{[Hf]} = \frac{1}{\omega_1} \cos^{-1}\left[\frac{(d_5 - d_1 d_4)\omega_1^2 - (d_2 + d_3)d_5}{d_5^2 + \omega_1^2 d_4^2}\right],$$

where $i\omega_1$ *is root of characteristic equation (8.22).*

Case (3): When τ_1 is fixed and τ_2 as a variable parameter

We consider equation (8.16) with τ_1 as fixed parameter and τ_2 as a variable. Let $i\omega$ be a root of characteristic equation (8.16). Then splitting real and imaginary parts, we obtain

$$d_4\omega\sin\omega\tau_2 + d_5\cos\omega\tau_2 = \omega^2 - d_2 - d_2\cos\omega\tau_1, \tag{8.23}$$

$$d_4\omega\cos\omega\tau_2 - d_5\sin\omega\tau_2 = -\omega d_1 + d_3\sin\omega\tau_1. \tag{8.24}$$

Squaring and then adding (8.23) and (8.24) to eliminate τ_2, we obtain

$$\omega^4 + (d_1^2 - d_4^2 - 2d_2)\omega^2 + (d_2^2 + d_3^2 - d_5^2) - 2\omega d_1 d_3\sin\omega\tau_1 + 2d_3(d_2 - \omega^2)\cos\omega\tau_1 = 0. \tag{8.25}$$

Equation (8.25) is a transcendental equation in complex form. So, it is not easy to predict the nature of roots. Without going detailed analysis, we assume that there exist at least one positive root ω^*. From equations (8.23) and (8.24) one can obtain

$$\tau_{2_n}^* = \frac{1}{\omega^*}\cos^{-1}\left[\frac{\omega^{*2}d_5 - d_2d_5 - d_3d_5\cos\omega^*\tau_1 - \omega^{*2}d_1d_4 + \omega^* d_3d_4\sin\omega^*\tau_1}{d_5^2 + d_4^2\omega^{*2}}\right] + \frac{2n\pi}{\omega^*}, \tag{8.26}$$

Now, to verify the transversality condition of Hopf-bifurcation, differentiating equation (8.23) and (8.24) with respect to τ_2 and substitute $\tau_2 = \tau_2^*$, we obtain

$$\begin{aligned} P_1\left[\frac{d(Re\ \xi)}{d\tau_2}\right]_{\tau_2=\tau_2^*} + Q_1\left[\frac{d\omega}{d\tau_2}\right]_{\tau_2=\tau_2^*} &= R, \\ -Q_1\left[\frac{d(Re\ \xi)}{d\tau_2}\right]_{\tau_2=\tau_2^*} + P_1\left[\frac{d\omega}{d\tau_2}\right]_{\tau_2=\tau_2^*} &= S, \end{aligned} \tag{8.27}$$

where

$$P_1 = d_1 - d_3\tau_1\cos\omega^*\tau_1 + d_4\cos\omega^*\tau_2^* - d_5\tau_2^*\cos\omega^*\tau_2^* - d_4\omega^*\tau_2^*\sin\omega^*\tau_2^*,$$

$$Q_1 = -2\omega^* - d_3\tau_1\sin\omega^*\tau_1 - d_5\tau_2^*\sin\omega^*\tau_2^* + d_4\sin\omega^*\tau_2^* + d_4\omega^*\tau_2^*\cos\omega^*\tau_2^*,$$

$$R = d_5\omega^*\sin\omega^*\tau_2^* - d_4\omega^{*2}\cos\omega^*\tau_2^* \text{ and } S = d_5\omega^*\cos\omega^*\tau_2^* + d_4\omega^{*2}\sin\omega^*\tau_2^*.$$

Solving equation (8.27) for $\left[\frac{d(Re\ \xi)}{d\tau_2}\right]_{\tau_2=\tau_2^*}$, it is obtained

$$\left[\frac{d(Re\ \xi)}{d\tau_2}\right]_{\tau_2=\tau_2^*,\ \xi=i\omega^*} = \frac{RP_1 - SQ_1}{P_1^2 + Q_1^2}.$$

Theorem 8.5.3. *For system (8.3), with fixed τ_1 and assuming $RP_1 - SQ_1 \neq 0$ holds, there exists a positive number τ_2^* such that system (8.3) undergoes a Hopf-bifurcation at $\tau_2 = \tau_2^*$.*

Case (4): When τ_2 is fixed and τ_1 as a variable parameter then under an analysis similar to Case (3), one can easily prove the following theorem.

Theorem 8.5.4. *For a fixed τ_2 the system(8.3) undergoes a Hopf-bifurcation at $\tau_1 = \tau_1^*$, given by*

$$\tau_1^* = \frac{1}{\omega_*}\tan^{-1}\left[\frac{d_1\omega_* + d_4\omega_*\cos\omega_*\tau_2 - d_5\sin\omega_*\tau_2}{\omega_*^2 - d_2 - d_4\omega_*\sin\omega_*\tau_2 - d_5\cos\omega_*\tau_2}\right],$$

where $i\omega_*$ is characteristic root of equation (8.16).

8.6 Computer simulations

In this particular section, we shall perform some simulations and depict graphs in favor of our analytic findings. These simulations are done using MATLAB R2020b with the following parametric values:

$$\begin{aligned} &r = 3.5, \quad r_0 = 0.5, \quad r_1 = 0.0375, \quad k = 1.8, \quad \mu = 0.2, \\ &\nu = 0.1, \quad a = 0.2, \quad c = 0.45, \quad \delta = 0.76, \quad \delta_1 = 0.025. \end{aligned} \tag{8.28}$$

For the above values of parameters, three equilibrium exist $E_0(0,0), E_*(80,0)$ and $E^*(8.60126, 1.13557)$. The trivial equilibrium point E_0 has eigenvalues -0.76 and 3. So, it is a saddle point. The axial equilibrium point E_* is also a saddle point as eigenvalues (-3 and 0.954286) have opposite sign. The positive equilibrium point E^* has eigenvalues $-0.042206 \pm 0.927918i$ with negative real part, so it is locally asymptotically stable. We observe that both the species oscillate around the equilibrium in transient state and as time passes they move towards their respective steady states. This nature demonstrates the local asymptotic stability of the unique positive equilibrium point. The stable behavior is depicted in figure 8.2.

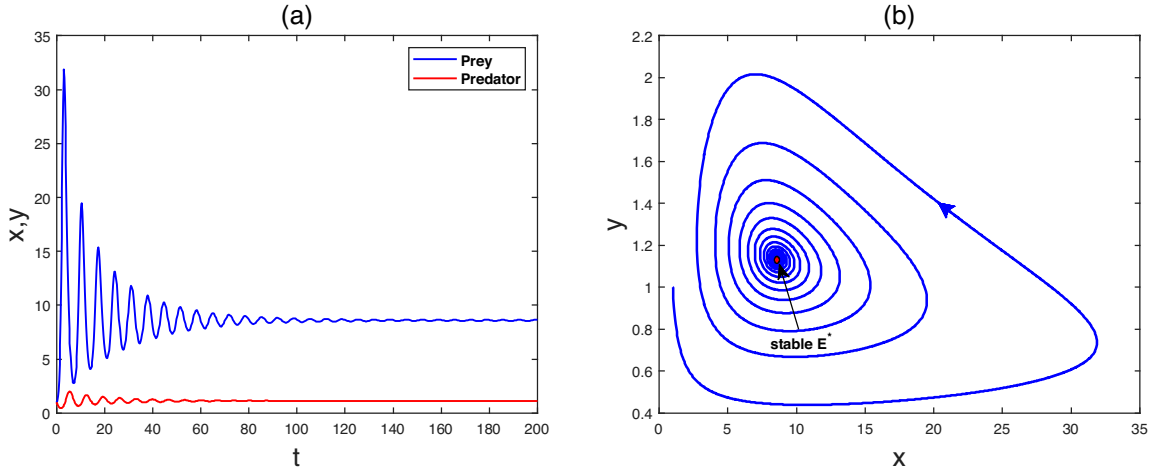

Fig. 8.2: Time series evolution of species and phase portrait for parametric set (8.28). The system (8.2) is locally asymptotically stable in a vicinity of the positive equilibrium point E^*.

It is observed that the transient period of both the species increases as we decrease the cost of fear k, and at a threshold value of k the system becomes unstable around the positive equilibrium point. The bifurcation point of parameter k is computed by equation (8.12) as $k^{[Hf]} = 0.987135$. Since $A_2 = 0.967012 > 0$ and $\frac{d}{dk}\Big(tr(J|_{E^*})\Big)\Big]_{k=k^{[Hf]}} = -0.77301 < 0$. Therefore, according to Theorem 8.4.6, system (8.2) experiences a Hopf-bifurcation with respect to parameter k at $k^{[Hf]} = 0.987135$. If we keep the cost of fear below this level then system shows its instability behavior and limit cycle appears in the phase portrait of the system. We also computed the value of σ^* using the formula given in [220]. The numerical value of σ^* is obtained as $\sigma^* = -0.507181$. Since $\sigma^* < 0$, so the Hopf-bifurcation is supercritical [169] and the limit cycle is stable in nature.

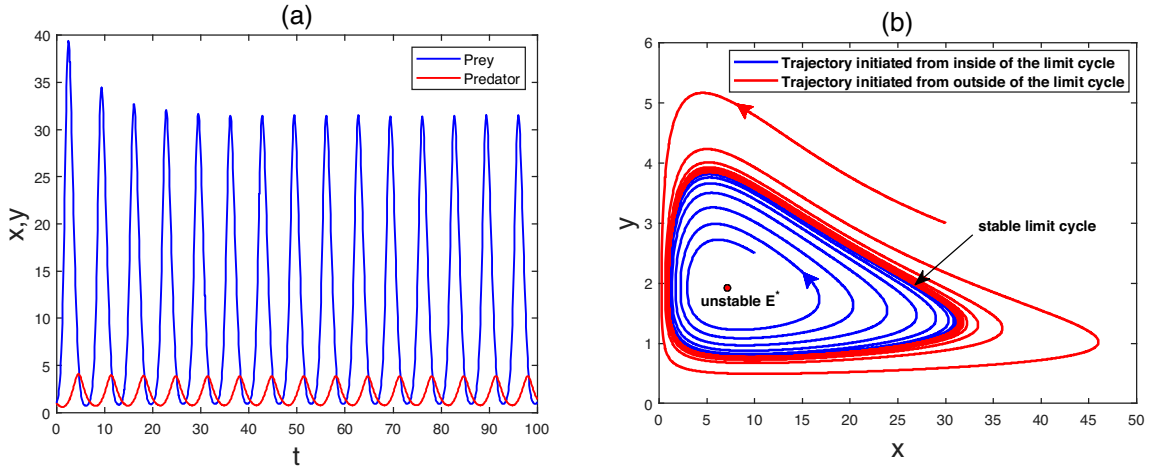

Fig. 8.3: Unstable nature of solutions and existence of stable limit cycle of system (8.2) around the positive equilibrium point E^* at $k = 0.5 < k^{[Hf]} = 0.987135$.

The unstable nature of the positive equilibrium is narrated graphically in figure 8.3. It can be noted that the solution trajectories oscillate around the positive equilibrium and converge to the limit cycle. To confirm the stability of the limit cycle, we initiated two solution trajectories from the inside (blue) and outside (red) of the cycle and perceived that both the trajectories are attracted by the limit cycle. This behavior of the limit cycle indicates its stable nature. The stability and instability of the system can be illustrated in a much better way by the bifurcation diagram (see Fig. 8.4). The blue and red curves show the upper peak and lower peak of the limit cycle for corresponding value of bifurcation parameter k. The difference between the blue and red curve exhibits the double amplitude of the limit cycle. From the figure 8.4, one can observe that the amplitude of the limit cycle decreases along the positive direction of k and vanishes at $k = k^{[Hf]}$ and remains zero for further increment in k. This demonstrates the presence of limit cycle before $k = k^{[Hf]}$ and stability of the positive equilibrium point for higher cost of fear.

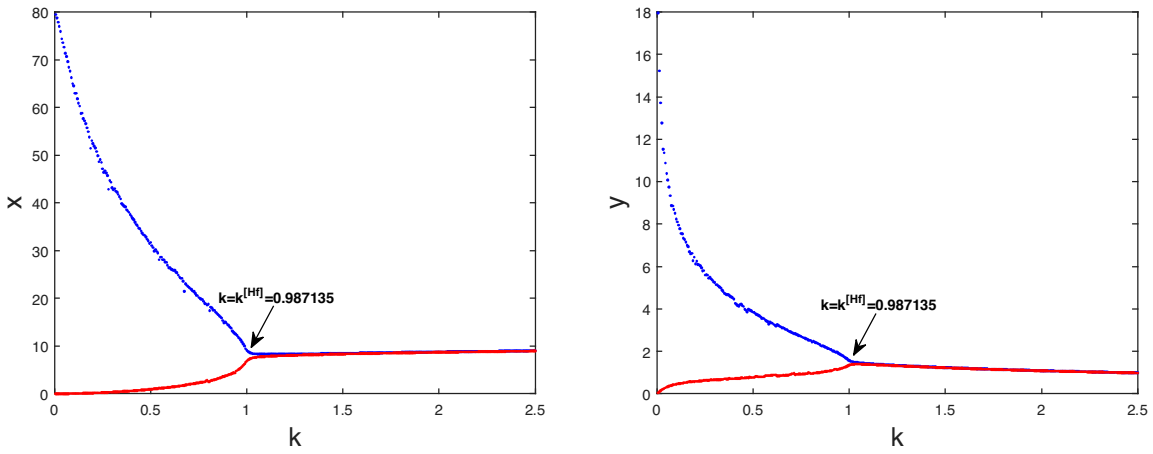

Fig. 8.4: Bifurcation diagram for x and y with respect to cost of fear k. The system is bifurcated from unstable equilibrium and stable limit cycle to stable equilibrium point at $k = k^{[Hf]} = 0.987135$.

The Hopf-bifurcation with respect to v is also identified. The threshold value of v is evaluated $v^{[Hf]} = 0.134875$. Therefore, the stability of positive equilibrium point will change as v crosses its threshold value and limit cycle is produced around the equilibrium point. Further, the stability and direction of bifurcation is verified by computing σ^* using the formula given in Wang et al. [220]. Since $\sigma^* = -1.032453 < 0$, so Hopf-bifurcation is supercritical and the limit cycle is stable. In figure 8.5, we plotted two solution trajectories for $v = 0.18 > v^{[Hf]}$. The blue trajectory is started from inside of the limit cycle and the red trajectory is started from outside of the limit cycle. Both the trajectories are attracted by the limit cycle which insures its stability.

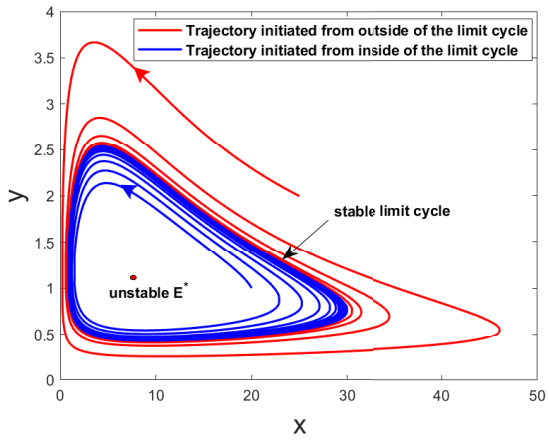

Fig. 8.5: Stable limit cycle when $\nu = 0.18$.

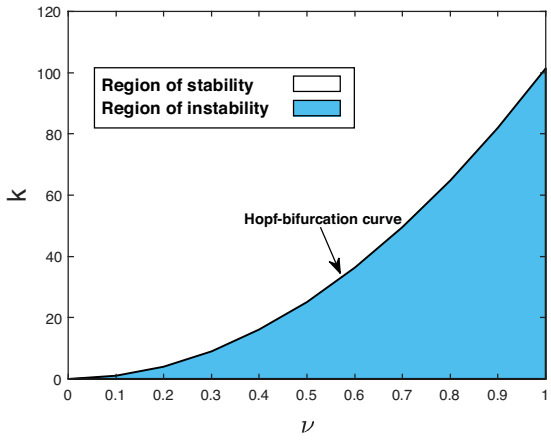

Fig. 8.6: Region of stability and instability in $\nu k-$ plane.

In the above discussion, we noted that the system (8.2) undergoes a supercritical Hopf-bifurcation in reference to parameters k and ν. Therefore, it is feasible to separate the $\nu k-$ plane into two regions viz, region of stability and region of instability (refer to Fig. 8.6). The unique positive equilibrium point is asymptotically stable in the white region, so it is called region of stability. On the other hand, stable periodic solution exists around unstable equilibrium point in the blue region, so it is called region of instability in the context of equilibrium point. Both the regions are separated by a curve. Each point on this curve is a Hopf-bifurcation point for corresponding values of ν and k (other values are same as in parametric set (8.28)). Hence, the separation curve is named Hopf-bifurcation curve.

To explore some more dynamical features for the model (8.2) like transcritical bifurcations, we pick out the following parametric set.

$$\begin{aligned} &r = 3.5, \quad r_0 = 0.5, \quad r_1 = 0.275, \quad k = 1.8, \quad \nu = 0.1, \\ &a = 0.2, \quad c = 0.45, \quad \delta = 0.76, \quad \delta_1 = 0.025. \end{aligned} \tag{8.29}$$

We take μ as a bifurcation parameter, for this set of parameters, $E_*(10.909091, 0)$ is the axial equilibrium point for all values of μ. Initially for very small values of μ, the positive equilibrium does not exist and in such a case E_* is locally asymptotically stable. Now we increase μ, then at $\mu = \mu^{[tc]} = 0.233781$, the positive equilibrium appears in the scenario. The axial equilibrium point E_* leaves its stability as soon as the positive equilibrium point E^* comes into existence. It sounds like the axial equilibrium handovers its stability to the positive equilibrium point for further values of μ. Again, we evaluate all $\Delta_i (i = 1, 2, 3)$ (refer to Theorem 8.4.8).

Our computation shows:

$$V = \begin{bmatrix} 1 \\ -1.776316 \end{bmatrix}, \quad W = \begin{bmatrix} 0 \\ 1 \end{bmatrix}, \quad \Delta_1 = 0, \quad \Delta_2 = -3.824096 \neq 0, \quad \Delta_3 = 1.036895 \neq 0.$$

Hence, as per Theorem 8.4.8, the system (8.2) experiences a transcritical bifurcation between the equilibrium points E_* and E^* with respect to parameter μ at $\mu^{[tc]} = 0.233781$. This characteristic of the system is described for both the species x (left) and y (right) by figure 8.7. The blue dashed and red dashed curves correspond to stable and unstable equilibrium point respectively. Moreover, if we increase the parameter μ, then the steady-state level of x falls down which is quite reasonable, if predators consume prey species with a higher attack rate then prey species will decrease. But the steady-state level of predators initially grows up to a certain value $(\mu \approx 1)$ and then starts decreasing. The reason is when predator consumes prey at a larger attack rate then over-exploitation of prey occurs and in consequences of that the prey starts fall off. The predators also go down due to lack of food resources. Now if we further increase the value of μ, then system becomes unstable and both the species start to fluctuate.

The system undergoes a Hopf-bifurcation with respect to μ at $\mu^{[Hf]} = 2.056025$ as shown in figure 8.7. The system is stable around its positive equilibrium point if $\mu^{[tc]} < \mu < \mu^{[Hf]}$ and becomes unstable as μ crosses $\mu^{[Hf]}$. Stable limit cycle arises in the system and unstable E^* is shown by red dashed curve inside the limit cycle in figure 8.7.

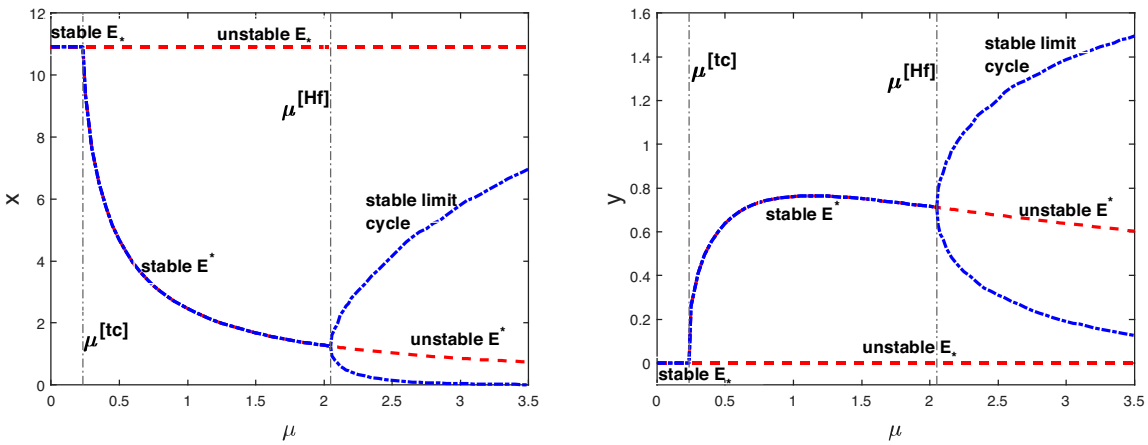

Fig. 8.7: Bifurcation diagram for both the species with respect to parameter μ. The system (8.2) shows transcritical bifurcation at $\mu = \mu^{[tc]} = 0.233781$ and Hopf-bifurcation at $\mu = \mu^{[Hf]} = 2.056025$. Other parameters are same as in (8.29).

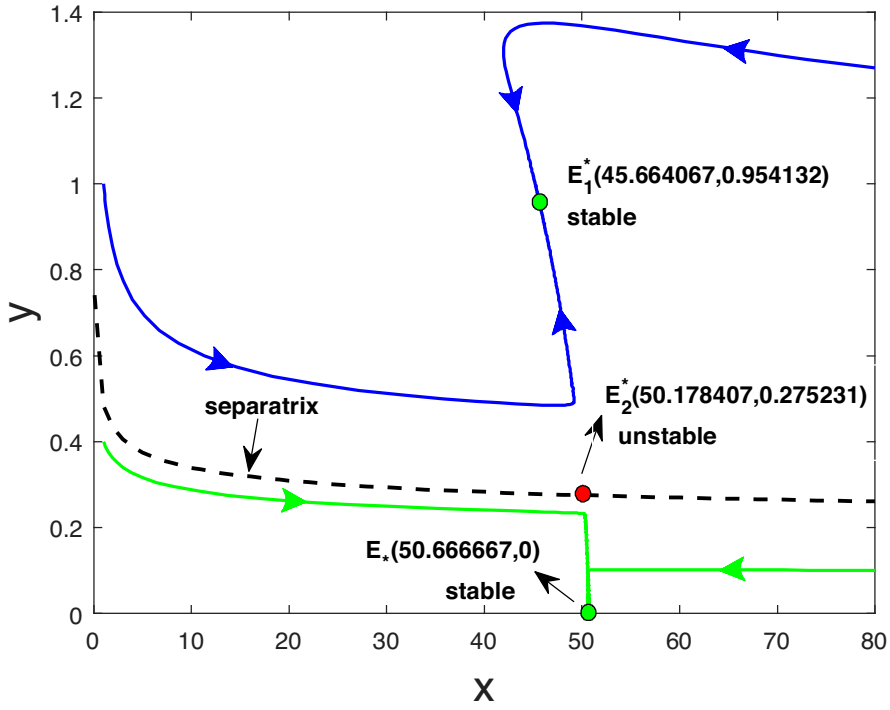

Fig. 8.8: Bi-stability phenomenon between equilibrium points E_1^* and E_* for the system (8.2). Parameters are chosen as in (8.30) and $\mu = 0.008$.

For the parametric set (8.30), we examined the following points:

- The system (8.2) does not have any positive equilibrium point when $\mu < \mu^{[sn]} = 0.007184$ while it has two positive equilibrium points E_1^* and E_2^* when $\mu > \mu^{[sn]} = 0.007184$. E_1^* is locally asymptotically stable and E_2^* is saddle point.

- The system (8.2) has an axial equilibrium point $E_*(50.666667, 0)$ for all values of parameter μ. From the inequality (8.8) we found that E_* is locally asymptotically stable when $\mu < 0.009445$ and saddle point when $\mu > 0.009445$.

These observations show that there are two locally asymptotically stable equilibrium points (E_* and E_1^*) when $0.007184 < \mu < 0.009445$. Hence the system (8.2) exhibits the bi-stability phenomenon for the parametric set (8.30) and $0.007184 < \mu < 0.009445$. In figure 8.8, we have plotted several trajectories for $\mu = 0.008$ from different initial pairs. The black dashed curve is separatrix, that separates basin of attraction of both locally asymptotically stable equilibrium points. It can be seen that two blue solution curves that are initiated from above of the separatrix, approach to the positive equilibrium point $E_1^*(45.664067, 0.954132)$ and green solution curves that are initiated from below of the separatrix, approach to the axial equilibrium $E_*(50.666667, 0)$.

Remark 8.6.1. *It is interesting to note here that the predator population extincts when the attack rate* $\mu < 0.007184$ *and coexists with prey when* $\mu > 0.009445$. *But when* $0.007184 > \mu > 0.009445$, *then the existence and extinction of predator population depend upon initial populations.*

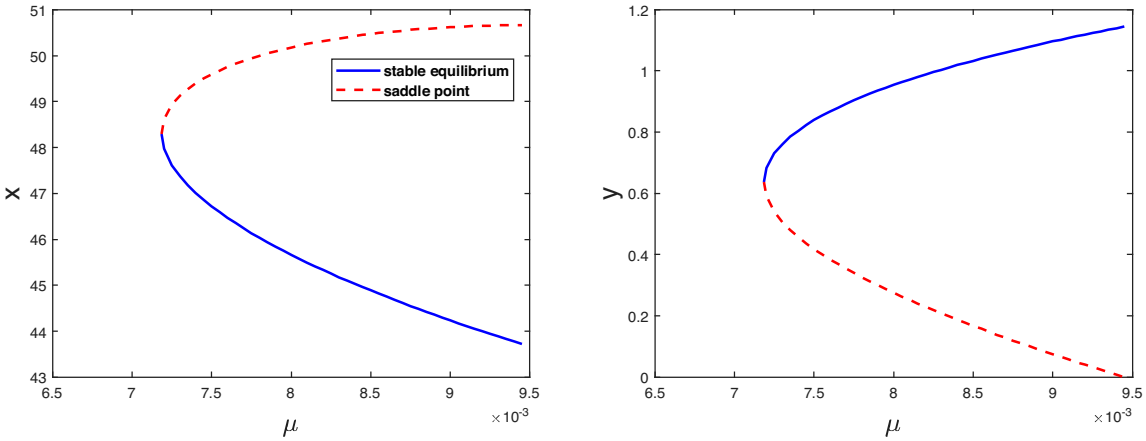

Fig. 8.9: Saddle node bifurcation diagram of system (8.2) with respect to μ, the solid curve stands for stable equilibrium and the dotted curve is stands for saddle point.

In order to show the saddle node bifurcation in system (8.2), we choose the parameters as follows:

$$\begin{aligned} &r = 2, \quad r_0 = 0.1, \quad r_1 = 0.0375, \quad k = 0.1, \quad \nu = 0.02, \\ &a = 0.2, \quad c = 0.43, \quad \delta = 0.1878, \quad \delta_1 = 0.25. \end{aligned} \tag{8.30}$$

For the above set of parameters the threshold value of μ, where $det(\bar{J}) = 0$ is obtained $\mu^{[sn]} = 0.007184$ and the interior equilibrium is $\bar{E} = (48.29704, 0.637887)$. The Jacobian of the system at $\bar{E}$ is given by

$$\bar{J} = \begin{bmatrix} -1.809419 & -12.61917 \\ 0.003846 & 0.026786 \end{bmatrix}.$$

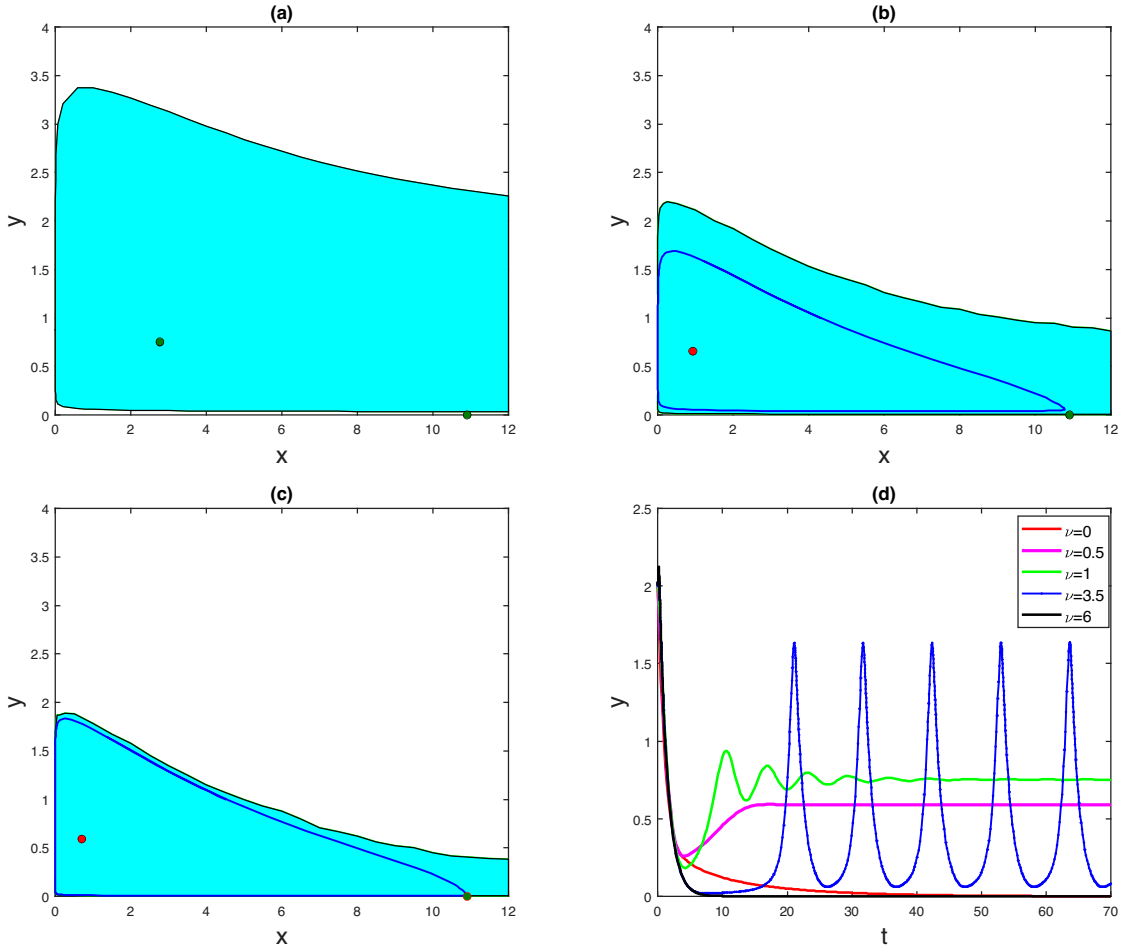

Fig. 8.10: (a-c) Separatrix and basin of attraction of equilibrium points E_* and E_1^* (or limit cycle around it) for different values of cooperation coefficient ν (a) $\nu = 1$, (b) $\nu = 4$, (c) $\nu = 6$. Basin of attraction of E_* is in white color and basin of attraction of E_1^* (or limit cycle) is in cyan color. Red dot denotes unstable equilibrium point while green dot denotes stable equilibrium point and blue curve in (b-c) is limit cycle. (d) Extinction and existence of predator for different values of parameter ν.

The eigenvectors corresponding to zero eigenvalue of $\bar{J}$ and $\bar{J}^T$ are calculated $V_1 = \begin{bmatrix} 1 \\ -0.143387 \end{bmatrix}$ and $W_1 = \begin{bmatrix} 1 \\ 470.51378 \end{bmatrix}$ respectively. We have $F_\mu(\bar{E}, \mu^{[sn]}) = \begin{bmatrix} -21.659878 \\ 9.313747 \end{bmatrix}$ and $D^2F(\bar{E}, \mu^{[sn]})(V_1, V_1) = \begin{bmatrix} -0.336037 \\ -0.0020163 \end{bmatrix}$. Transversality conditions for saddle-node bifurcation are given by

$$\Omega_1 = W_1^T F_\mu(\bar{E}, \mu^{[sn]}) = 4360.586625 \neq 0 \text{ and } \Omega_2 = W_1^T D^2F(\bar{E}, \mu^{[sn]})(V_1, V_1) = -1.284729 \neq 0.$$

Thus, from the Sotomayor's Theorem [169] the system (8.2) undergoes a saddle node bifurcation around $\bar{E} = (48.29704, 0.637887)$ at $\mu = \mu^{[sn]} = 0.007184$. This particular bifurcation has

also been illustrated geometrically in figure 8.9.

In figure 8.9, it can be seen that there are two interior equilibrium points E_1^* and E_2^* coexist for higher values of parameter μ. E_1^* is stable node whereas E_2^* is saddle point. Now if we alleviate the value of μ both the equilibrium points come towards each other and at the threshold value $\mu = \mu^{[sn]} = 0.007184$ they collide and annihilate each other via a saddle node bifurcation. None of the interior equilibrium exists for $\mu < \mu^{[sn]}$.

Now, we consider on parametric set (8.29) to examine the effect of cooperation coefficient. For this, we fix $\mu = 0.2$ and vary the parameter ν. It is noticed that the axial equilibrium point $E_*(10.909091, 0)$ is stable for all ν. Initially, when $\nu = 0$, then system does not have any positive equilibrium point. Therefore, species will approach E_*. This shows that predator population extincts when there is no cooperation among them while hunting. On increasing ν, at $\nu = 0.2918$, two positive equilibrium E_1^* (stable node) and E_2^* (saddle point) appear in the system via a saddle node bifurcation. Since E_* is always stable, so the system shows bistablity between E_* and E_1^*. In figure 8.10(a), basin of attraction of E_* and E_1^* are presented in phase plane of x and y. This shows that coexistence or extinction of predator depends upon initial conditions. At $\nu = 1.3$, the system undergoes a local Hopf-bifurcation and species start oscillate. For $\nu > 1.3$, the system shows bi-stability between E_* and the stable limit cycle around E_1^*. The basin of attraction of E^* and limit cycle are drawn in figure 8.10(b). On further increasing ν, the period of limit cycle increases and its basin of attraction shrinks (see figure 8.10(c)). This indicates that the possibility of coexistence of species falls off with further increment in ν. In figure 8.10(d), we have plotted time evolution curves of predator population for different values of ν. All the solution curves are started from same initial pair (1,2). It can easily be noted that when $\nu = 0$, predator vanishes after a certain time, when $\nu = 0.5$ and 1, predator attains its steady state level, when $\nu = 3.5 > 1.3$, predator population oscillates and when $\nu = 6$, predator population goes for extinction.

In order to employ the numerical simulation of delayed system (8.3), we choose the value of parameters given in the set (8.28). The numerical values of equilibrium points remain same as earlier. The set of inequalities in (8.10) also holds, that shows initially the system is stable around the positive equilibrium point E^* in the absence of both the delay parameters. From equation (8.19), we get the unique positive value of ω_0 which is 0.926686. Further, we obtain the critical value of τ_1 which is $\tau_1^{[Hf]} = 0.112093$ with the help of formula derived in (8.21). Since $h'(\omega_0^2) = 1.507833 \neq 0$, so the transversility condition also holds. Hence, according to Theorem 8.5.1, the delayed system (8.3) experiences a Hopf-bifurcation near E^* at $\tau_1 = \tau_1^{[Hf]} = 0.112093$.

In the figure 8.11, time evolution of species (left) and the phase portrait (right) are presented for $\tau_1 = 0.08 < \tau_1^{[Hf]}$. We see that the solution curve approaches towards E^* with time and eventually stabilizes on E^*. This behavior of E^* demonstrates its local asymptotic stability. If

we increase the value of τ_1 beyond its critical value $\tau_1^{[Hf]}$, then the system becomes unstable near E^* via a Hopf-bifurcation and a limit cycle arises. The unstable behavior is depicted in the figure 8.12 for $\tau_1 = 0.13 > \tau_1^{[Hf]}$.

To experience the Hopf-bifurcation in a different perspective, we plot the bifurcation diagram (refer to Fig. 8.13). In this diagram, we have plotted only attractors for different values of delay parameter τ_1. It can be observed that when $\tau_1 < \tau_1^{[Hf]}$ the trajectories are attracted by the positive equilibrium point E^*, which also insures the stable nature of E^* and when $\tau_1 > \tau_1^{[Hf]}$ then the trajectories are attracted by stable limit cycles, drawn in the figure 8.13.

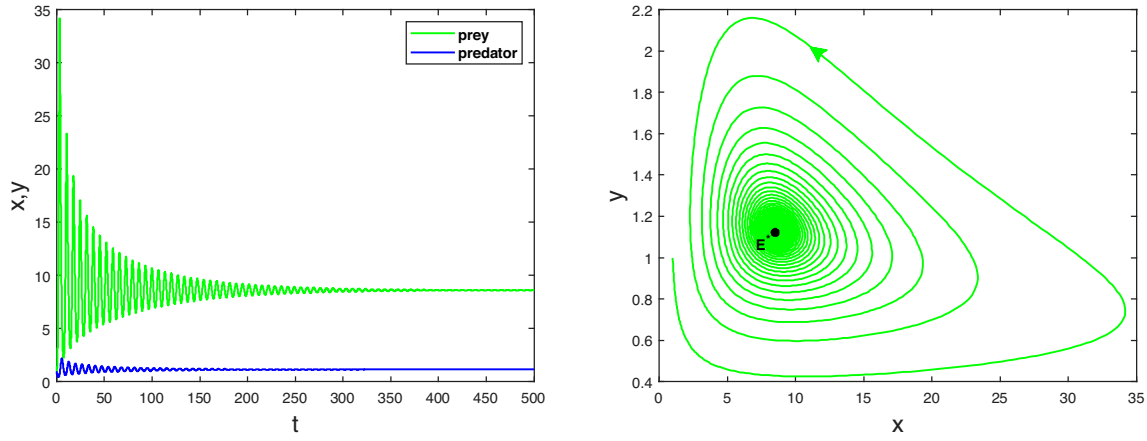

Fig. 8.11: Time series evolution of species (left) and phase portrait (right) at $\tau_1 = 0.08 < \tau_1^{[Hf]}$. The system (8.3) is locally asymptotically stable near the positive equilibrium point E^*.

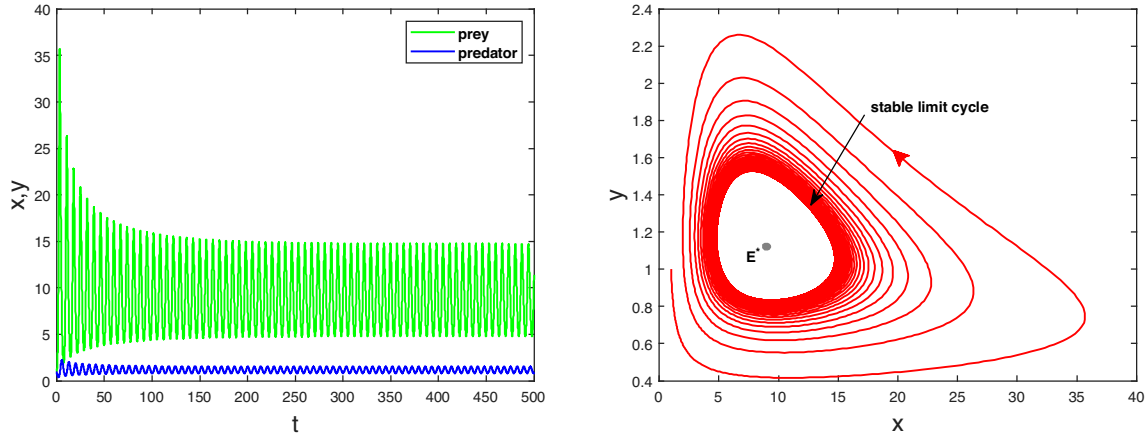

Fig. 8.12: Unstable nature of solutions and existence of stable limit cycle of system (8.3) around the positive equilibrium point E^* at $\tau_1 = 0.13 > \tau_1^{[Hf]}$.

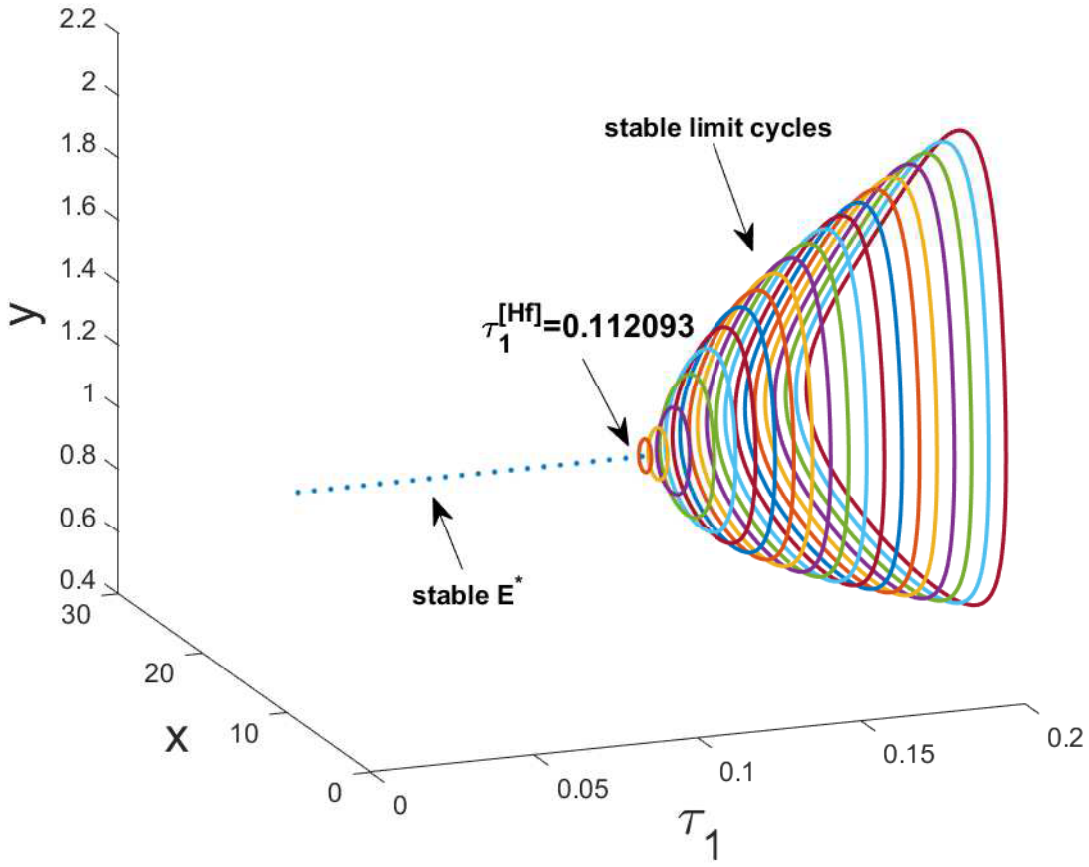

Fig. 8.13: Bifurcation diagram with respect to delay parameter τ_1. The system is bifurcated from stable equilibrium to unstable equilibrium point and stable limit cycle at $\tau_1 = \tau_1^{[Hf]} = 0.112093$.

As the delayed system (8.3) exhibits Hopf-bifurcation with respect to parameters k and τ_1, we can bisect the $k\tau_1-$ plane into following two regions keeping other parameters same as in (8.28).

Region of stability (green) $S_1 = \{(k, \tau_1)$: system (8.3) is locally asymptotically stable near $E^*\}$,

Region of instability (white) $S_2 = \{(k, \tau_1)$: system (8.3) is unstable$\}$.

Both the regions are drawn in figure 8.14. It is noted that the threshold value of delay parameter $\tau_1^{[Hf]}$ increases with cost of fear k and vice versa. The curve which separates both the regions is called Hopf-bifurcation curve.

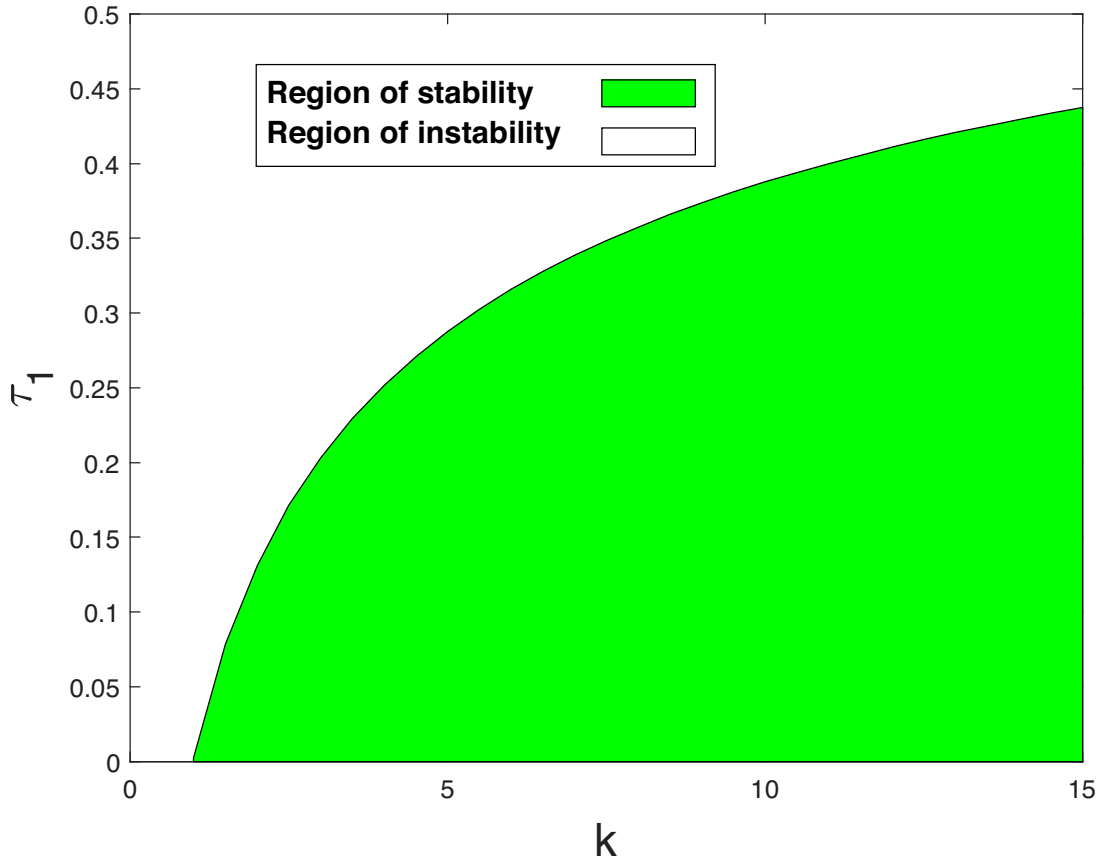

Fig. 8.14: Region of stability and instability of the system (8.3) in $k\tau_1$−plane. Other parameters are same as in (8.28).

Now if $\tau_1 = 0$ and $\tau_2 > 0$, then there does not exist any purely imaginary root of the characteristic equation (8.22) for the parametric set (8.28). Therefore, the system (8.3) will never change its stability status on varying τ_2. As the set of inequalities in (8.10) holds and non-delayed system is stable with parameters in (8.28). Hence, the delayed system is stable around its positive equilibrium for all values of τ_2. Nevertheless, to explore some more characteristics of the delayed system, we change numerical values of some parameters like $k = 1$ and $r_1 = 0.00375$. Due to this change in parameters the axial and positive equilibrium point shift at $(800, 0)$ and $(7.54079, 1.670848)$ respectively. In this case the inequalities in (8.10) do not hold and hence the non-delayed system is no longer stable. The equation (8.22) has purely imaginary root when $\tau_2 = \tau_2^{(1)} = 2.62025$ and $\tau_2 = \tau_2^{(2)} = 4.423719$. Therefore, the system (8.3) undergoes a local Hopf-bifurcation twice at $\tau_2^{(1)} = 2.62025$ and $\tau_2^{(2)} = 4.423719$. Initially when $\tau_2 = 0$ system is unstable around E^* and remains unstable up to $\tau_2^{(1)}$ whereas it is stable between $\tau_2^{(1)}$ and $\tau_2^{(2)}$. The system changes its stability again at $\tau_2^{(2)}$ and falls into instability for all further values of τ_2.

In the range of delay $7.3 < \tau_2 < 10.5$, the system goes through period-doubling oscillations, which often sounds like a route to chaos. The system behaves as a chaos and shows sensitivity with respect to initial pair at higher values of $\tau_2(\tau_2 > 11.4)$. In figure 8.15, we plotted two solutions starting from two nearby initial pairs for $\tau_1 = 18$ and notified that a slightest difference of 0.0001 in initial values causes a significant difference between both the solutions at a finite time. This shows the chaotic nature of the system. The strange behavior of both the species is depicted as a phase portrait in figure 8.16. To see the behavior of the system for a wide range of τ_2, we draw the bifurcation diagram (refer to Fig. 8.17) that demonstrates the system from periodic oscillations to chaotic nature via period-doubling bifurcation.

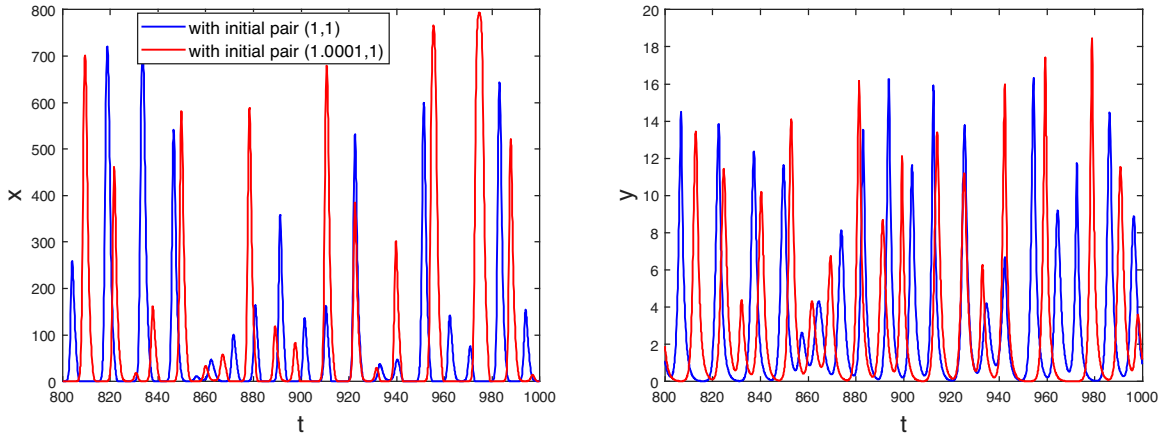

Fig. 8.15: Sensitivity of solutions of system (8.3) with respect to initial condition when $\tau_2 = 18$.

The fact that the system is chaotic for a wide range of the delay parameter does not mean that chaos is the same in each case, even chaoticity can be quantified and that can be reflected in the complexity of the time series. To analyze the quantity of chaos, we calculate and map maximum Lyapunov exponent (Fig. 8.18) and Poincare sections (Fig. 8.19) for various values of τ_2. Lyapunov exponent refers that how sensitive a system is with respect to initial conditions. Positive (negative) Lyapunov exponent indicates that the system is chaotic (non-chaotic). A positive but small Lyapunov exponent points out that the system is chaotic but less sensitive with respect to initial conditions. In figure 8.18, graph stays negative until $\tau_2 = 11.4$ and then it rises above zero that confirms the chaotic regime of the system.

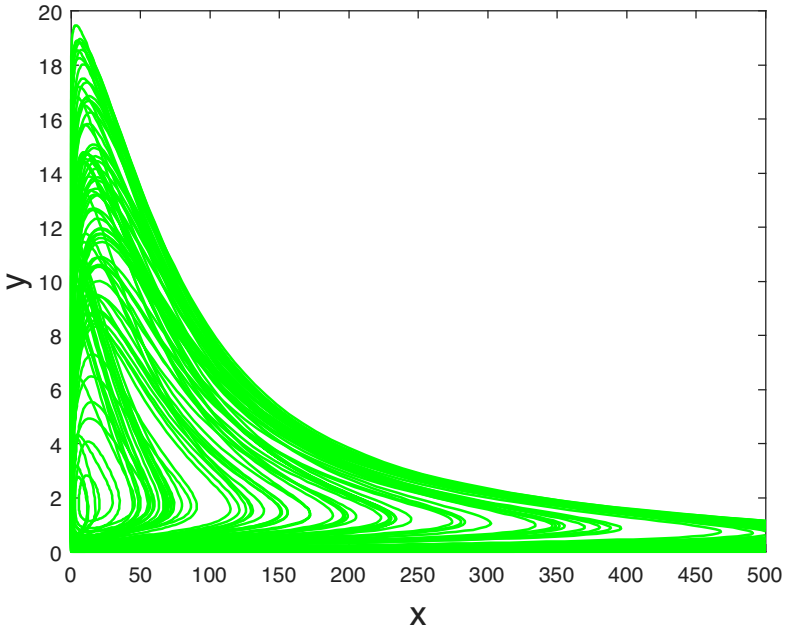

Fig. 8.16: Stranger attractor at $\tau_2 = 18$.

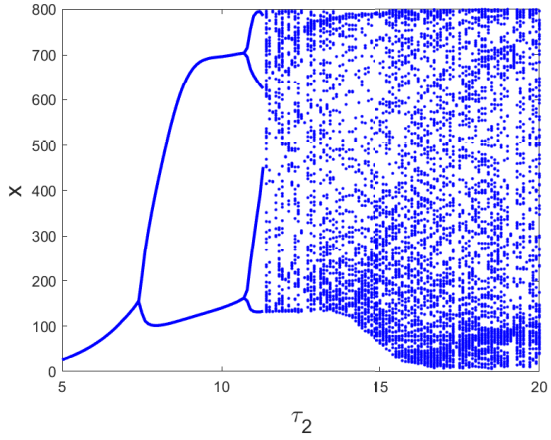

Fig. 8.17: Bifurcation diagram of system (8.3).

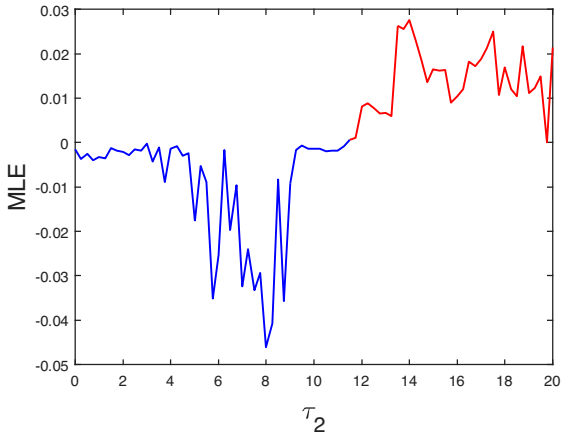

Fig. 8.18: Maximum Lyapunov exponent of system (8.3).

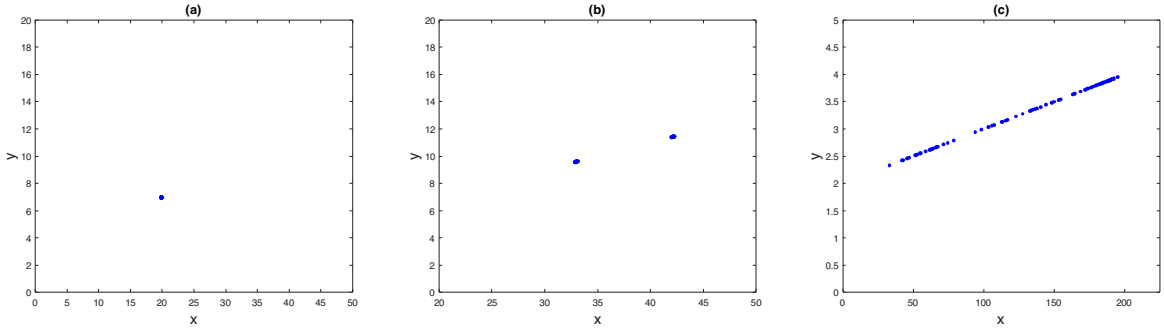

Fig. 8.19: Poincare sections of system (8.3) for different values of τ_2. When $\tau_2 = 6$, limit cycle exists in the system (a), the system have period doubling solutions at $\tau_2 = 10$ (b), when $\tau_2 = 18$, system shows higher periodic (chaotic) oscillation (c).

Here we have done some simulations on case (3) of the delayed system (8.3) keeping $\tau_1 = 0.25$ fixed and τ_2 as a variable parameter for the parametric values given in set (8.28). We noticed stability behavior of the system on varying the delay parameter τ_2 in a wide range. Initially when $\tau_2 = 0$, the system is unstable around E^* as $\tau_1^{Hf} < 0.25$. From the formula (8.26) given in the previous section, we obtain six different values of τ_2. The obtained critical values of τ_2 are $1.183063, 5.025491, 8.58355, 11.233724, 15.984048, 17.441955$, where system experiences local Hopf-bifurcations (refer to Theorem 8.5.3) i.e. system becomes unstable to stable at $\tau_2 = 1.183063$ and becomes stable to unstable again at $\tau_2 = 5.025491$ and so on. We have shown the unstable nature and stable nature for $\tau_2 = 1 < 1.183063$ and $1.183063 < \tau_2 = 4 < 5.025491$ of the system respectively in figure 8.20. The multiple switching is an important characteristic of the system in view of ecology as the stability of the system directly dependent upon the time taken in group forming by predators. The stability switching behavior of species can be seen in bifurcation diagram 8.21. From figure 8.21, it can be seen that the stability change via hopf-bifurcation occurs exactly six times at the obtained critical values of parameter τ_2.

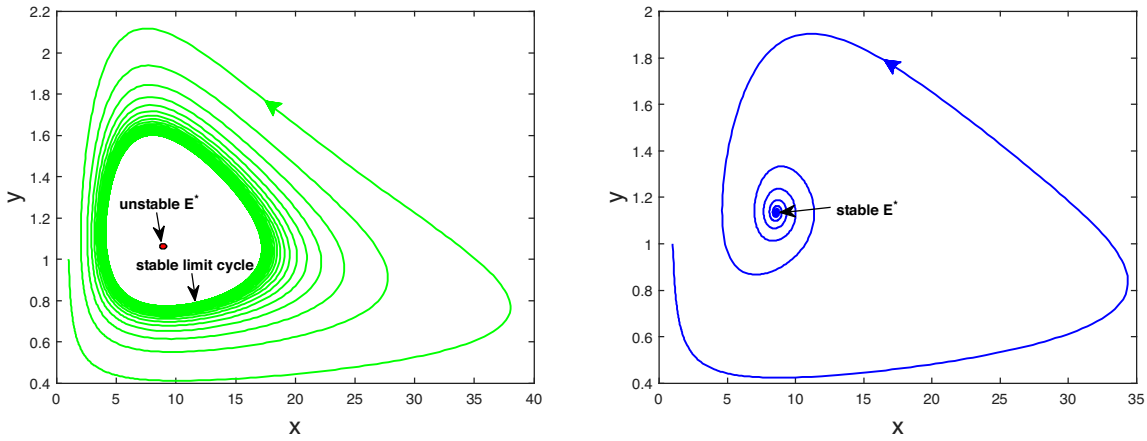

Fig. 8.20: Presence of a stable limit cycle when $\tau_2 = 1 < 1.183063$ (left) and stable phase diagram at $1.183063 < \tau_2 = 4 < 5.025491$ (right) when $\tau_1 = 0.25$ is fixed.

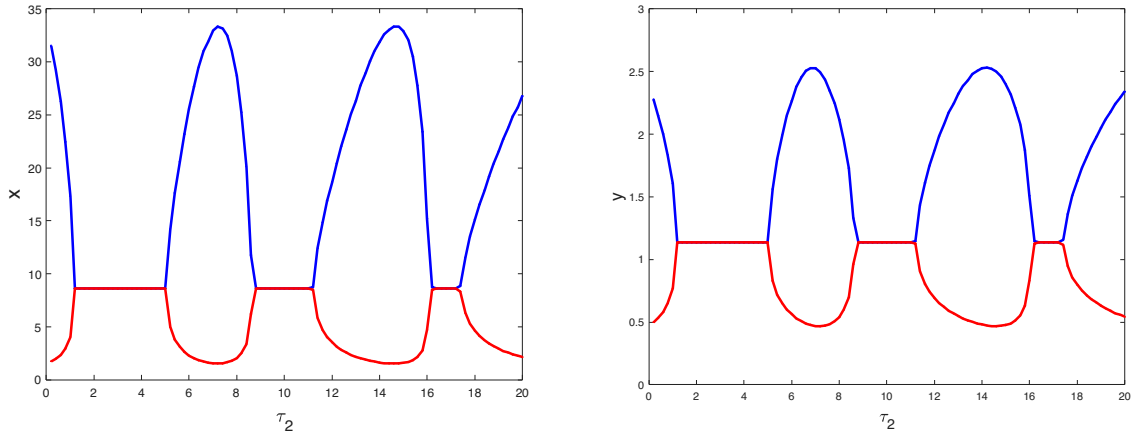

Fig. 8.21: Bifurcation diagram of delayed system (8.3) with respect to τ_2 when $\tau_1 = 0.25$ is fixed.

Now we consider the case (4) when $\tau_2 = 6$ is fixed and τ_1 is a variable parameter. According to formula obtained in Theorem 8.5.4 and choosing the parametric set (8.28), our computer simulation yields

$$\omega_* = 0.969397 \text{ and } \tau_1^* = 0.128111.$$

The transversality condition also holds, therefore according to the Andronov Hopf Theorem, system (8.3) undergoes a Hopf-bifurcation with respect to τ_1 at τ_1^*. Initially when $\tau_1 = 0$ system is stable near E^*. Now if we increase τ_1 then remains stable till $\tau_1 = \tau_1^*$ and then it becomes unstable via Hopf-bifurcation on more increment in parameter τ_1 (see Fig. 8.22). In figure 8.23, we have separated the $\tau_2\tau_1-$plane into two regions, viz. region of stability and region of instability. From the figure, it can be noted that if τ_1 is fixed in $(0.112, 0.636)$ then the system

switches its stability multiple times with respect to τ_2 but if τ_1 lies away from this range then the system does not change its stability even once and the behavior remains same for all τ_2.

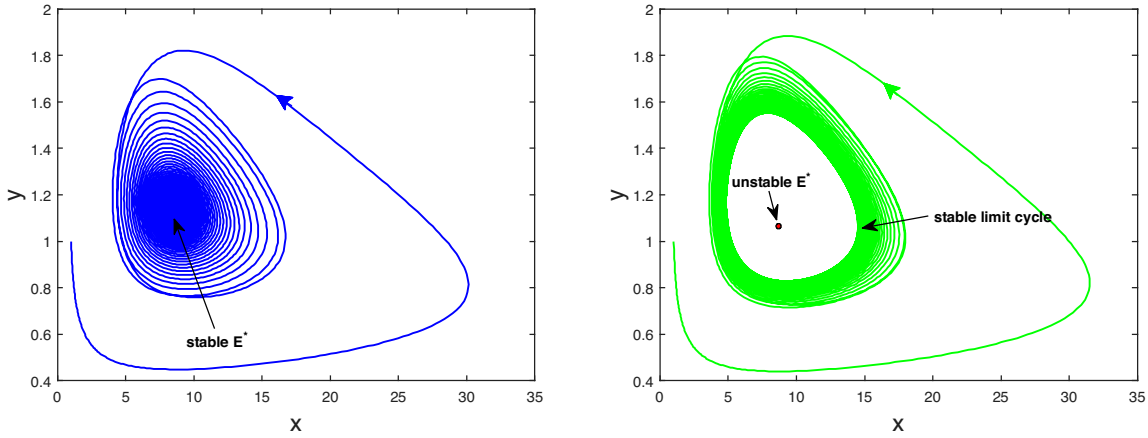

Fig. 8.22: Phase portrait of system (8.3) when $\tau_1 = 0.1 < 0.128111$ (left) and presence of a stable limit cycle at $\tau_1 = 0.15 > 0.128111$ (right) when $\tau_2 = 6$ is fixed.

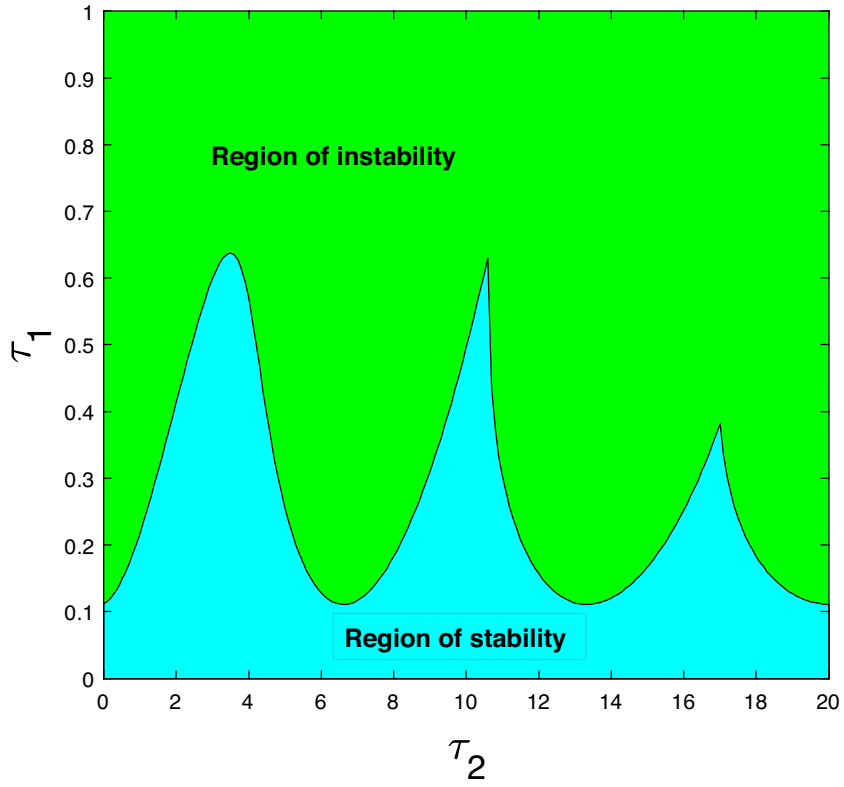

Fig. 8.23: Region of stability and instability of the system (8.3) in $\tau_2\tau_1-$plane. Other parameters are same as in (8.28).

Remark 8.6.2. *In case (2) (when $\tau_1 = 0$ and $\tau_2 \neq 0$), it has been observed that the system shows chaotic behavior for some parametric values ($r_1 = 0.00375$, $k = 1$ and other parameters are same as in (8.28)). This chaotic nature can be controlled from the system by introducing anti-predation response delay τ_1 (see figure 8.24).*

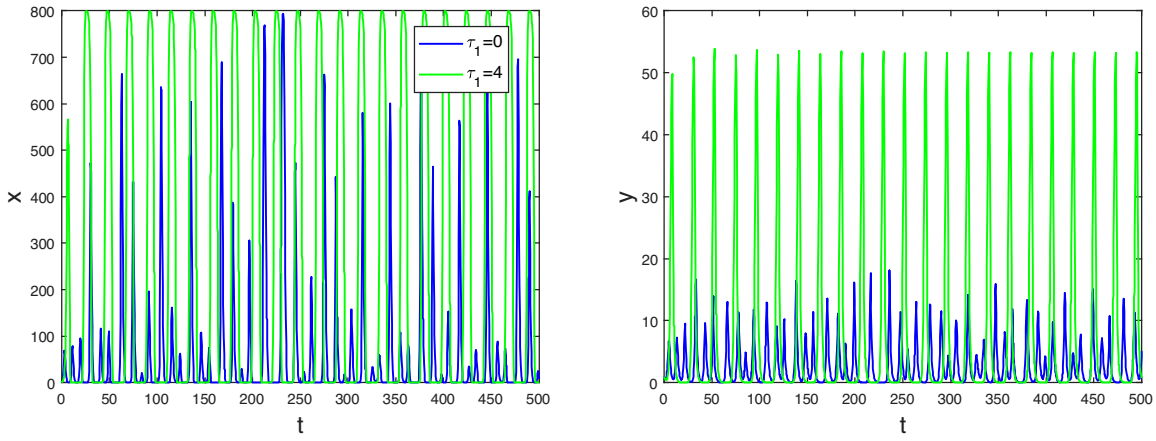

Fig. 8.24: Time series evolution for two different value of τ_1 when $\tau_2 = 18$. The figure shows that uneven oscillations can be controlled by increasing τ_1.

8.7 Conclusion

Due to universal existence and significance in many multispecies systems, group hunting is a concern of exploration among theoretical ecologists over a long span. Although, a few studies have been conducted on group hunting by the mathematical modelling approach but still less attention is paid [7, 178, 162]. On the other hand, direct killing is the pillar at which the prey-predator relationship is hinged. But in recent studies, it is investigated that predator induces fear as well in prey individuals and because of this, their reproduction rate falls off [220]. The separation of fear effect from direct killing by predators was being possible just because of the tremendous experimental work by several theoretical ecologists [236, 201]. In the present chapter, we deal with a prey-predator model with fear effect in prey population by predator individuals and cooperation among predator individuals while hunting. Further, we incorporate two discrete delays taken into account of time lags in anti-predation response due to fear and delay in cooperation. The prey population is growing logistically in absence of predators but in the presence of predators, they remove prey by direct killing and reduce their birth rate by inducing fear as well. We modified fear function that affects prey population in a more realistic way and to include the effect of team hunting, we use Berec's approach.

The model shows complex and varied dynamical behavior. The solutions of the system are positive and bounded in a positive invariant set Ω. We have examined the persistence of

the model that gives two parametric conditions for the coexistence of both the species for all future time. It is noted that if the birth rate of prey r is bigger enough than a threshold and the natural death rate of predator δ is less than another threshold, then both the species will survive evermore. We analyzed that how the number of interior steady state and there stability nature vary with change in parameters. The local stability of all existing equilibrium is investigated and obtained parametric conditions under with the system is stable around them. The trivial equilibrium point is always a saddle point so the system never collapses for any value of parameters. Since, the condition of stability of the axial equilibrium E_1 and the positive equilibrium E^* are not exclusive and overlap for a certain range of parameter μ, therefore the system shows bi-stability between E_1 and E^*. For the chosen set of parameters in (8.30), and $0.007184 < \mu < 0.009445$, the existence of predator population depends on initial conditions.

The model experiences various bifurcations such as saddle-node, transcritical and Andronov Hopf with respect to different parameters. Since the predator population depends only on hunting prey individuals. Therefore, predators are absent from the system (or E_1 is stable) at low attack rate μ. For any set of parameters, there is a threshold value of μ ($\mu^{[tc]}$) where E_1 transfers its stability to E^* and predator population comes into the scenario. The cost of fear plays a vital role in the complex dynamics of the system. It is capable to remove chaotic oscillations from the system and the oscillations are further controlled through Hopf-bifurcation on increasing the cost of fear. The effect of strength of cooperation and cost of fear is also explored in νk bi-parametric plane keeping other parameters fixed. It is interesting to see that the Hopf-bifurcation value of k increases quadratically with ν (refer to Fig. 8.6). We noted that the strength of cooperation among predators is as crucial as their attack rate. For a chosen set of parameters, predators will die out if they do not cooperate while hunting. If we increase ν, then a stable positive equilibrium point appears via saddle-node bifurcation and the species coexist. On further increment in ν, the basin of attraction of E^* shrinks and the possibility of coexistence falls off (refer to Fig. 8.10). This shows that the higher cooperative strength of predators while hunting leads to their extinction. This is because of the fact that higher cooperation among predators reduces the density of prey species.

We have explored the dynamics of the model by incorporating two discrete delays; one is anti-predation response delay (τ_1), in order to delay in response to the induced fear by predators and another is cooperation delay (τ_2), representing the time lag in forming group and preparation for the attack. The incorporation of delays does not affect the equilibria of the system so the number of equilibria and their value remains as it is in the delayed system. We found that the Jacobian matrix of the system at E_0 and E_1 remains same as the non-delayed system. Hence, the local behavior of both the equilibrium points is not affected by the delay. So, basically, our main aim is to analyze the stability and Hopf-bifurcation of the system in the vicinity of E^* for both the delays.

We have considered all the possible cases with both the delays. First we assumed that $\tau_2 = 0$ and obtained a critical value of τ_1 (8.21), where the system leaves stability and attains limit cycle via Hopf-bifurcation (see Fig. 8.13). The dynamics is further studied in $k\tau_1$ bi-parameter plane and observed that the bifurcation value $\tau_1^{[Hf]}$ increases with cost of fear k. In the case of $\tau_1 = 0$, system does not change its stability for all $\tau_2 > 0$. So, we replace $r_1 = 0.00375$ and $k = 1$. For these values, the characteristic equation has two roots. So the stability changes twice. On the large values of delay parameter ($\tau_2 > 11.4$), chaotic nature is detected. Moreover, the chaotic behavior of the delayed system is confirmed by evaluating maximum Lyapunov exponent and mapping Poincare sections (refer to Figs. 8.18 and 8.19). Ecologically, if predators spend more time in forming groups against prey (it may happen due to miscommunication or lack of coordination among individuals), then both the population oscillate in a strange manner and become sensitive with respect to their initial populations. The bi-parametric analysis is carried out in $\tau_1\tau_2$ plane and interestingly we get a non-monotonic Hopf-bifurcation curve in the plane (see Fig. 8.23). This shows the bubbling phenomenon occurs in the system when $0.112 < \tau_1 < 0.636$. In this range of τ_1, stability of the system switches multiple times on varying τ_2. It is observed that if $\tau_1 = 0.25$ then system shows cyclic behavior and populations reach periodic oscillation around E^* for $\tau_2 = 0$. On increasing τ_2, system undergoes Hopf-bifurcation six times and eventually attains the cyclic behavior for all larger τ_2. Generally, stability switching in a delayed system through Hopf-bifurcation can be justified by its memory. In this case when stability of the system switches multiple times, it happens possibly due to recollection of its memory [162].

Lastly, we have conclude that fear induced by predators is capable to reduce the oscillations of the system and plays an important role in the stabilization of the ecosystem. Cooperation while hunting is an essential characteristic of predator individuals that plays a vital role in their survival. Apart from this, both the delays make the model dynamics richer and more extensive.